Joint Deployment and Resource Allocation for Service Provision in Multi-UAV-Assisted Wireless Networks

Shengqi Geng, Zhe Wei, Jian Zhao, *Senior Member, IEEE*, Furao Shen, *Member, IEEE*, Jingon Joung, *Senior Member, IEEE*, and Sumei Sun, *Fellow, IEEE*

***Abstract*—There has been a growing interest in using unmanned-aerial-vehicles (UAVs) for high-rate wireless communications due to their flexibility in deployment and relatively low costs. In this article, we consider an UAV-assisted wireless network, where a multiantenna ground base station provides communication services to a group of users through a set of UAVs using the in-band wireless backhaul. We propose a novel framework for optimizing the multi-UAV-assisted wireless network and consider the following two problems: one minimizes the total system cost and the other maximizes the system utility. In contrast to the previous studies, we consider the deployment cost of UAVs and the impact of the UAV locations on the backhaul capacity for both the problems. The two problems are complicated mixed-integer nonlinear programming (MINLP) problems, which involve the joint optimization of the UAV selection and their locations, the UAV-user association, and the wireless resource allocations subject to the Quality of Service requirements of users and the wireless backhaul capacity constraints. Therefore, we propose the block coordinate descent-based algorithms combined with successive convex approximation to solve the two problems. Simulation results show that the proposed methods are adaptable to the wireless backhaul constraints and outperform the other benchmark methods.**

***Index Terms*—Mixed-integer nonlinear programming (MINLP), unmanned-aerial-vehicle (UAV) communications, UAV deployment, wireless backhaul.**

Manuscript received 3 June 2024; revised 6 July 2024; accepted 5 August 2024. Date of publication 13 August 2024; date of current version 7 November 2024. This work was supported in part by the SRIBD Innovation Fund under Grant SIF20240012; in part by the Jiangsu Provincial Key Research and Development Program under Grant BE2023031; and in part by the National Natural Science Foundation of China under Grant 62276127. The work of Jingon Joung was supported in part by the National Research Foundation of Korea (NRF) Grant funded by the MSIT under Grant 2022R1A2C1003750 and Grant RS-2024-00405510. This article was presented in part at the IEEE International Conference on Communications, Denver, CO, USA, June 9–13, 2024. *(Corresponding authors: Jian Zhao; Furao Shen.)*

Shengqi Geng, Zhe Wei, and Jian Zhao are with the School of Electronic Science and Engineering, Nanjing University, Nanjing 210023, China (e-mail: shengqi_geng@smail.nju.edu.cn; virgilwei6365@gmail.com; jianzhao@nju.edu.cn).

Furao Shen is with the State Key Laboratory for Novel Software Technology and the School of Artificial Intelligence, Nanjing University, Nanjing 210023, China (e-mail: frshen@nju.edu.cn).

Jingon Joung is with the School of Electrical and Electronics Engineering, Chung-Ang University, Seoul 06974, South Korea (e-mail: jgjoung@cau.ac.kr).

Sumei Sun is with the Institute for Infocomm Research, Agency for Science, Technology, and Research, Singapore 138632 (e-mail: sunsm@i2r.a-star.edu.sg).

Digital Object Identifier 10.1109/JIOT.2024.3443125

I. Introduction

UNMANNED-AERIAL-VEHICLES (UAVs) have a diverse range of applications in various sectors, including telecommunications, rescue operations, surveillance, and package delivery. They have received considerable research interest in the recent years [1], [2], [3]. UAVs are expected to play a crucial role in the future wireless networks to enhance the communication capacity and coverage [4], [5], [6]. Compared to the conventional terrestrial communications, UAV-assisted wireless communications offer two main advantages. First, the availability of Line of Sight (LoS) air-to-ground (A2G) channels between the user equipment (UE) and UAVs helps to mitigate the signal blockage [7]. Second, the locations of UAVs can be chosen flexibly, allowing for increased flexibility in their deployment. For example, the terrestrial wireless networks in remote regions with sparsely deployed ground base stations (GBSs) may be inadequate to meet the communication requirements. In such scenarios, cost-effective UAV-assisted wireless networks can be practical solutions [8], [9]. UAVs are also critical in providing emergency connectivity to the wireless devices in disaster areas where the conventional cellular coverage is unavailable.

UAVs can serve as static aerial base stations for the wireless services by hovering over the selected locations. Various studies have investigated UAV-assisted wireless networks with diverse objectives, such as maximizing ground-UE coverage [10], optimizing average data rate under worst-case bit error rate constraints [11], and enhancing energy efficiency [12]. However, deploying many UAVs to provide the wireless services can incur significant investment costs for the network providers. Furthermore, the wireless backhaul capacity between the UAVs and the GBS is a limiting factor that determines the system performance, which also depends on the number and location of the deployed UAVs [13]. Therefore, it is crucial to consider the tradeoff between the system throughput and the UAV deployment cost in the multi-UAV-assisted wireless networks. This article presents a novel framework to optimize the multi-UAV-assisted wireless networks, addressing the research challenge of efficient UAV deployment while considering the impact of the UAV locations on the backhaul capacity and the associated deployment costs. We focus on jointly optimizing the UAV selection,

UAV locations, UAV-UE association, and wireless resource allocation to enhance the overall network performance.

A. Related Work

In UAV-assisted wireless networks, the positions of UAVs and the allocation of communication resources are crucial for enhancing the network performance. Several studies have investigated their joint optimization. Mahmood et al. [14] proposed an efficient algorithm for determining the allocation of radio resources, 3-D placement of UAVs, and UE association matrices in an orthogonal frequency division multiple access (OFDMA)-enabled UAV-assisted communication system to provide on-demand services. Lin et al. [15] proposed a dynamic UAV deployment approach to optimize the UAV locations for enlarging the UE coverage and reducing the communication energy consumption. Chen et al. [16] proposed an approach to maximize the energy efficiency of device-to-device (D2D) pairs in an UAV-enabled wireless network by jointly optimizing the power control, channel allocation, and UAV deployment while ensuring the secrecy rates for all the UEs. Leveraging the game theory and the matching theory, Lhazmir et al. [17] proposed a novel framework to analyse the associations between the UAVs and the Internet of Things (IoT) devices, optimizing the assignment of suitable UAVs for energy-efficient and load-balanced data collection from the ground IoT networks. Huo et al. [18] introduced an UAV-enabled hierarchical distributed learning architecture for the machine learning applications, which employed a two-sided many-to-one matching game to determine the optimal association between the UAV transmitters and receivers. Zhou et al. [19] proposed a clustering-aided reinforcement learning approach to maximize the sum rates among all the ground users within a limited power budget by jointly optimizing user association and power control in an UAV-assisted network.

Existing studies have also considered optimizing the placement of a given set of UAVs in a wireless network for the service provision. For example, Kang et al. [20] investigated the deployment of UAV relays between the source and destination nodes, where they proposed using the Gibbs sampling method to determine the UAV locations. In [21], a distributed learning method was proposed to jointly optimize the placement and power allocation of multiple UAVs in an unknown region, with the aim to maximize the sum of α-fairness for all UEs. The MeanShift clustering method was employed in [22] to address the 2-D UAV positioning and UAV-UE association problem. One of the benefits is that the MeanShift clustering method does not require the number of UAVs to be determined in advance; instead, it obtains the number of UAVs according to the clustering result. Sun and Masouros [23] proposed a naive successive deployment method and a clustering-based method to maximize the UE coverage and power efficiency. In addition, Wang et al. [24] proposed a centralized multiagent Q-learning algorithm for the UAV deployment and UAV-UE associations in an UAV-assisted cellular network to minimize the power consumption during the uplink transmission. The aforementioned studies considered deploying a predetermined number of UAVs in the network. In practical scenarios, the UE requirements cannot be adequately met if the number of deployed UAVs is insufficient. On the other hand, deploying too many UAVs wastes system resources and may cause severe interference in the network. Therefore, it is also crucial to determine the required number of UAVs to meet the communication requirements while considering the associated cost.

Another important issue to be addressed in UAV-assisted communication networks is the limited capacity of the wireless backhaul that connects the UAVs to the GBS [25]. Du et al. [26] investigated the resource allocation for the backhaul in a cellular UAV network to maximize the aggregate energy efficiency of the system. Hu et al. [27] considered the in-band wireless backhaul and maximized the uplink throughput by jointly optimizing the UAV altitude, power control, and bandwidth allocated between the backhaul and access links. Other studies, such as [28] and [29], used the K-means clustering method to find the 2-D placement of UAVs and adjusted the UAV-UE associations under the backhaul constraints using the heuristic methods. Qiu et al. [30] converted a sum-rate-utility maximization problem with backhaul constraints into an unconstrained problem and solved it using a gradient descent method. Banagar and Dhillon [31] evaluated the performance of a 3-D two-hop cellular network that uses GBS and UAVs to serve ground UEs, taking into account the realistic antenna radiation patterns for backhauling. In general, the wireless backhaul capacity in UAV-assisted networks is susceptible to the locations of UAVs and the propagation environment. Furthermore, the number of deployed UAVs is closely tied to the backhaul capacity, making it difficult to optimize the UAV deployment and wireless resource allocation jointly.

It is evident that the clustering methods have inherent drawbacks when determining the UAV deployments. The clustering methods are primarily based on the geographic distribution of UEs, which lead to wastage of the system resources when the UEs are dispersed. Meanwhile, the clustering methods deploy a single UAV at the centroid of each cluster, which may not maximize the sum rate of UEs or meet the Quality of Service (QoS) requirements. Additionally, positioning UAVs such that all the UEs are equidistant from the UAVs can result in varying communication rates due to the co-channel interference. Therefore, a more practical formulation should be developed to jointly consider the number and placement of UAVs, backhaul capacity, and QoS requirements for efficient resource allocation in the multi-UAV communication networks.

B. Research Gaps and Contributions

Existing research lacks adequate consideration for the cost of UAV deployment, which involves determining the appropriate number of UAVs in the network. Furthermore, the previous studies have often overlooked important factors, such as the number and locations of UAVs on the wireless backhaul capacity. Such oversights may result in unmet user requirements, inefficient resource utilization, or increased

network interference. To address these research gaps, we develop a comprehensive framework that jointly optimizes the UAV selection, UAV deployments, UAV-UE association, and wireless resource allocations. Our approach explicitly takes into account the required number of UAVs, their corresponding positions, and the impact of deployment strategies on the backhaul capacity.

We consider the joint optimization of UAV deployment and resource management in a multi-UAV-assisted wireless network, where the UAVs are connected to the GBS through the wireless backhaul. Each ground UE has its QoS requirement, and the backhaul capacity depends on the number of deployed UAVs, UAV locations, and the propagation environment. We consider the following two problems: one minimizes the total system cost and the other maximizes the system utility. Our formulation accommodates both the backhaul capacity constraints and the UE QoS requirements. For both the problems, the deployment cost of UAVs is considered. The two problems are complicated mixed-integer nonlinear programming (MINLP) problems, which involve the selection of UAVs and their locations, the UAV-UE associations, and the allocation of wireless resources (i.e., the transmit power of each UAV and the fraction of bandwidth allocated for each UE). The main contributions of this study are summarized as follows.

1) We address the practical and challenging problems that jointly optimize the selection and placement of UAVs and the allocation of wireless resources, subject to the QoS requirements of UEs and the wireless backhaul capacity constraints. To the best of our knowledge, no existing literature provides solutions for this complicated joint UAV deployment and resource optimization problem.
2) We present a novel framework that considers the system cost or the system utility for the service provision in multi-UAV-assisted wireless networks. The optimization problems consider the UAV selection, UAV placement, UAV-UE association, and wireless resource allocation to minimize the system cost or maximize the system utility of the wireless network composed of multiple UAVs. Unlike the commonly used clustering approach, our study considers the impact of the UAV locations on both the backhaul capacity and the UE transmission rates.
3) To address the challenging MINLP problems, we propose an effective solution approach that combines the block coordinate descent (BCD) with successive convex approximation (SCA) techniques [32] as shown in Fig. 1. Simulation results verify that the proposed algorithms have well-defined convergence properties and significantly outperform the other benchmark methods.

The remainder of this article is organized as follows. In Section II, the system model is introduced. Section III provides the problem formulation and the solution algorithm for minimizing the total system cost. The problem formulation and solution for maximizing the total system utility are provided in Section IV. Extensive simulations comparing the proposed algorithms with the benchmark methods are presented in Section V. Finally, conclusions are drawn in Section VI.

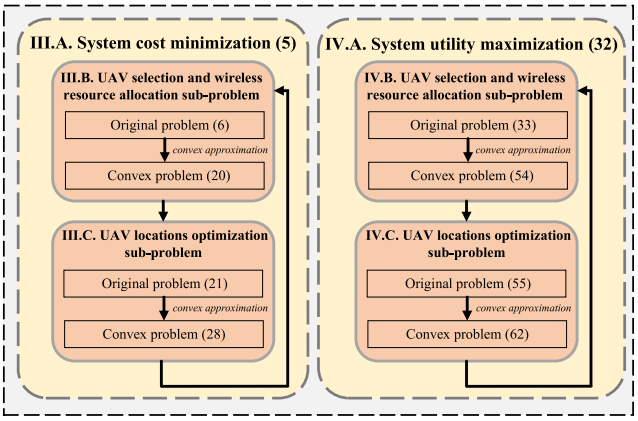

Fig. 1. Overview of the proposed algorithms.

TABLE I
LIST OF KEY NOTATIONS

Category	Description
Sets	
$\mathcal{K}$	The set of all UEs
$\mathcal{K}_j$	The subset of UEs served by the jth UAV
$\mathcal{J}$	The set of all UAVs
Parameters	
K	The number of all UEs
J	The number of all UAVs
β	The bandwidth allocation coefficient
B	The total system bandwidth
Γ_k	The QoS requirement of the kth UE
N_{T}	The antenna array size of the GBS
γ	The backhaul channel attenuation factor
P_0	The transmit power of the GBS
ρ_0	The channel power gain
z_0	The altitude of the GBS
$\mathbf{u}_0$	The 3D location vector of the GBS
σ_j^2	The Gaussian noise power at the jth UAV
σ_k^2	The Gaussian noise power at the kth UE
ξ_1	The pathloss coefficient for backhaul links
ξ_2	The pathloss coefficient for access links
$u_{j,\max}^z$,$u_{j,\min}^z$	The maximum/minimum altitude of the jth UAV
$p^{\max}$	The maximum transmit power of UAV
C_j	The backhaul capacity between the GBS and the jth UAV
Variables	
$\mathbf{a}$	The on/off state vector for all UAVs
a_j	The on/off state of the jth UAV
$\mathbf{u}_j$	The 3D location vector of the jth UAV
$\hat{\mathbf{u}}_k$	The 3D location vector of the kth UE
$\mathbf{p}$	The transmit power vector of all UAVs
p_j	The transmit power of the jth UAV
$\mathbf{X}$	The association matrix between the UEs and the UAVs
x_{kj}	The association between the kth UE and the jth UAV
$\mathbf{F}$	The fraction of bandwidth matrix between UEs and UAVs
$\mathbf{f}_k$	The bandwidth allocation vector for the kth UE
f_{kj}	The fraction of bandwidth occupied by the kth UE from the jth UAV
$\mathbf{b}$	The number of UEs vector served by all UAVs
b_j	The number of UEs served by the jth UAV
$\bar{\mathbf{r}}$	The data rate vector of UEs
$\bar{r}_k$	The data rate of the kth UE
d_j	The distance between the GBS and the jth UAV
d_{kj}	The distance between the kth UE and the jth UAV
G_{kj}	The average channel gain between the kth UE and the jth UAV

Notation: We use boldface lower- and upper-case letters to denote the vectors and matrices, respectively. The function $\log(\cdot)$ denotes the logarithm to the base 2. $\|\cdot\|$ denotes the ℓ_2 norm of a vector. $(\cdot)^{\mathrm{T}}$ denote the transpose of a vector or a matrix. $x^{(t)}$ denotes the value of the variable x in the tth

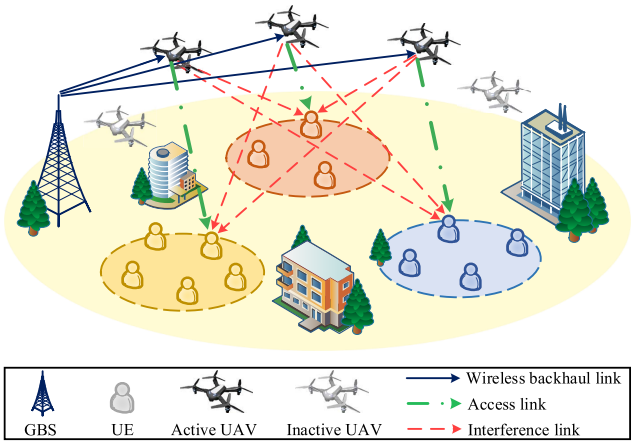

Fig. 2. Multi-UAV-assisted wireless network.

iteration. For a continuously differentiable function $f(x)$, $\nabla f(x)$ and $\nabla^2 f(x)$ denote the first- and second-order derivatives of $f(x)$, respectively. Table I summarizes the notations in this article.

II. System Model

We consider a wireless network assisted by a set of UAVs as shown in Fig. 2, where a multiantenna GBS provides communication services to a group of UEs in a disaster area via the UAVs. It is assumed that a large pathloss exists between the GBS and the UEs because the local GBSs are nonoperational due to the disaster, necessitating the use of the remote GBS to provide emergency communications. Here, the GBS first transmits the UE data to the UAVs through in-band wireless backhaul, and then the UAVs act as small-cell base stations to provide the data services to the UEs, which is addressed as the downlink transmission scenario. The number of UAVs is at most J, and there are K UEs in the network. We denote the set of available UAVs as $\mathcal{J} = \{1, \ldots, J\}$ and the set of UEs as $\mathcal{K} = \{1, \ldots, K\}$, respectively. Herein, the main objective is to choose an effective subset of the available UAVs to deploy in the network. To this end, we introduce a binary variable a_j to denote the on/off state of the jth UAV, where $a_j = 1$ if the jth UAV is chosen to be active, and $a_j = 0$ otherwise. The UAVs in the off-state do not need to be actually deployed, and the number of active UAVs in the network can be expressed as $\sum_{j\in\mathcal{J}} a_j$.

A. Wireless Backhaul Links

We use an in-band wireless backhaul for sending the data from the GBS to the UAVs. The total system bandwidth is B. The fraction of the total bandwidth allocated for the wireless backhaul is denoted as β, where $0 < \beta < 1$. Thus, the access link occupies $1-\beta$ of the total bandwidth. The GBS has a large antenna array with N_{T} antennas, whereas each UAV has one antenna. When the GBS simultaneously serves N_{g} UAVs using the zero-forcing scheme, where $N_{\mathrm{T}} \gg N_{\mathrm{g}}$, the beamforming gain can be calculated as $[(N_{\mathrm{T}} - N_{\mathrm{g}} + 1)/N_{\mathrm{g}}]$ [33], [34]. The backhaul links predominantly experience the LoS propagation paths. Taking into account the oxygen absorption and rain attenuation in the propagation model [35], [36] and considering that the GBS simultaneously serve $\sum_{j\in\mathcal{J}} a_j$ UAVs now, the wireless backhaul signal-to-interference-plus-noise ratio (SINR) at the jth active UAV can be well approximated as [34]

$$\mathrm{SINR}_{j,\mathrm{backhaul}} = \left(\frac{N_{\mathrm{T}}+1}{\sum_{j\in\mathcal{J}} a_j} - 1\right) \frac{P_0\rho_0}{d_j^{\xi_1}\sigma_j^2 10^{\gamma d_j/10}} \tag{1}$$

where P_0 is the transmit power of the GBS, σ_j^2 denotes the power of the additive white Gaussian noise (AWGN) at the jth UAV, γ is the channel attenuation factor due to the oxygen absorption and rain attenuation in dB/km, $d_j = \|\mathbf{u}_j - \mathbf{u}_0\|$ denotes the distance between the GBS and the jth UAV, ξ_1 is the pathloss coefficient between the GBS and the UAVs, and ρ_0 is the channel gain at a reference distance. Due to the fact that $([(N_{\mathrm{T}}+1)/(\sum_{j\in\mathcal{J}} a_j)] - 1)[(P_0\rho_0)/(d_j^{\xi_1}\sigma_j^2 10^{\gamma d_j/10})] \gg 1$, the backhaul capacity between the GBS and the jth UAV can be calculated as [34]

$$\begin{aligned} C_j(\mathbf{u}_j, \mathbf{a}) &= \beta B \log\left(1 + \mathrm{SINR}_{j,\mathrm{backhaul}}\right) \\ &\approx \beta B \log\left(\left(\frac{N_{\mathrm{T}}+1}{\sum_{j\in\mathcal{J}} a_j} - 1\right) \frac{P_0\rho_0}{d_j^{\xi_1}\sigma_j^2 10^{\gamma d_j/10}}\right) \end{aligned} \tag{2}$$

where $\mathbf{a} = [a_1, \ldots, a_J]^{\mathrm{T}}$. Note that, d_j in (2) is a function of $\mathbf{u}_j$.

B. Access Links

The 3-D locations of the GBS, the jth UAV and the kth UE are denoted by $\mathbf{u}_0 = [0, 0, z_0]^{\mathrm{T}}$, $\mathbf{u}_j = [u_j^x, u_j^y, u_j^z]^{\mathrm{T}}$ and $\hat{\mathbf{u}}_k = [\hat{u}_k^x, \hat{u}_k^y, 0]^{\mathrm{T}}$, respectively. Here, the jth UAV occupies a subregion that satisfies $\mathbf{u}_{j,\min} \le \mathbf{u}_j \le \mathbf{u}_{j,\max} \quad \forall j$, where $\mathbf{u}_{j,\min} = [u_{j,\min}^x, u_{j,\min}^y, u_{j,\min}^z]^{\mathrm{T}}$ and $\mathbf{u}_{j,\max} = [u_{j,\max}^x, u_{j,\max}^y, u_{j,\max}^z]^{\mathrm{T}}$. The jth UAV serves a subset of UEs denoted by $\mathcal{K}_j$, where $\mathcal{K}_j \subseteq \mathcal{K}$ and $\mathcal{K}_j \cap \mathcal{K}_{j'} = \emptyset$ if $j \neq j'$. Following the approach in [37] and [38], we assume that LoS signals predominantly influence the communication links between the UAVs and the UEs. Under this assumption, the average channel gain between the jth UAV and the kth UE can be calculated as $G_{kj} = \rho_0/d_{kj}^{\xi_2}$, where $d_{kj} = \|\mathbf{u}_j - \hat{\mathbf{u}}_k\|$ denotes the distance between the jth UAV and the kth UE, ξ_2 denotes the pathloss coefficient between the UAVs and the UEs, and ρ_0 denotes the channel power gain at the reference distance.

We introduce a binary variable x_{kj} to indicate the UAV-UE association, where $x_{kj} = 1$ if the kth UE is connected to the jth UAV, and $x_{kj} = 0$ otherwise. Hence, the SINR at UE $k \quad \forall k \in \mathcal{K}$, can be expressed as

$$\mathrm{SINR}_k(\mathbf{U}, \mathbf{X}, \mathbf{p}) = \frac{\sum_{j\in\mathcal{J}} x_{kj} p_j G_{kj}}{\sum_{j\in\mathcal{J}} (1 - x_{kj}) p_j G_{kj} + \sigma_k^2} \tag{3}$$

where $\mathbf{U} = [\mathbf{u}_1, \ldots, \mathbf{u}_J]$ denotes the location matrix of all the UAVs; $\mathbf{p}$ denotes the power allocation vector, whose jth element p_j is the transmit power of the jth UAV; and $\mathbf{X}$ denotes the association matrix whose (k, j)th element is x_{kj}; σ_k^2 denotes the noise power at the kth UE. In (3), $\sum_{j\in\mathcal{J}} x_{kj} p_j G_{kj}$ represents the received signal power at UE k from its associated UAV, whereas $\sum_{j\in\mathcal{J}} (1 - x_{kj}) p_j G_{kj}$ represents the interference caused by the other nonassociated UAVs.

We assume all the active UAVs use the same access spectrum to serve their UEs, and the UEs connected to the same UAV are allocated orthogonal channels using an OFDMA scheme to avoid the intrasubregion interference. The fraction of bandwidth occupied by UE k is denoted as f_{kj} if $k \in \mathcal{K}_j$. We have $f_{kj} \in (0, 1]$ if $k \in \mathcal{K}_j$. If UE k is not associated with the jth UAV, we set $f_{kj} = 0$. For each UAV, we have $\sum_{k\in\mathcal{K}_j} f_{kj} \leq 1 \quad \forall j$. Thus, the data rate for UE $k \quad \forall k \in \mathcal{K}$, can be calculated as [39]

$$R_k(\mathbf{U}, \mathbf{X}, \mathbf{p}, \mathbf{f}_k) = (1-\beta)B\left(\sum_{j\in\mathcal{J}} f_{kj}\right)\log(1+\mathrm{SINR}_k(\mathbf{U}, \mathbf{X}, \mathbf{p})) \tag{4}$$

where $\mathbf{f}_k = [f_{k1}, \ldots, f_{kJ}]^{\mathrm{T}}$ denotes the bandwidth allocation vector of the kth UE.

III. System Cost Minimization

The overall system cost in a multi-UAV-assisted wireless network comprises both the wireless communication cost and the cost associated with the UAV deployments. In this section, we consider the system cost minimization problem and propose its solution.

A. Optimization Problem Formulation

We model the system cost in a multi-UAV-assisted wireless network as a weighted sum of the wireless communication cost and the UAV deployment cost. The transmit power of the UAVs determines the wireless communication cost, whereas the UAV deployment cost is determined by the number of UAVs deployed in the network. Therefore, the system cost minimization problem can be formulated as

$$\min_{\{\mathbf{U},\mathbf{F},\mathbf{X},\mathbf{p},\mathbf{a}\}} \sum_{j\in\mathcal{J}} p_j + \lambda_1 \sum_{j\in\mathcal{J}} a_j \tag{5a}$$

$$\text{s.t.} \quad R_k(\mathbf{U}, \mathbf{X}, \mathbf{p}, \mathbf{f}_k) \geq \Gamma_k \quad \forall k \in \mathcal{K} \tag{5b}$$

$$\sum_{k\in\mathcal{K}} x_{kj}\Gamma_k \leq C_j(\mathbf{u}_j, \mathbf{a}) \quad \forall j \in \mathcal{J} \tag{5c}$$

$$0 \leq p_j \leq a_j p^{\max} \quad \forall j \in \mathcal{J} \tag{5d}$$

$$\sum_{j\in\mathcal{J}} x_{kj} = 1 \quad \forall k \in \mathcal{K} \tag{5e}$$

$$x_{kj} \leq a_j \quad \forall k \in \mathcal{K}, j \in \mathcal{J} \tag{5f}$$

$$f_{kj} \leq x_{kj} \quad \forall k \in \mathcal{K}, j \in \mathcal{J} \tag{5g}$$

$$\sum_{k\in\mathcal{K}} f_{kj} \leq a_j \quad \forall j \in \mathcal{J} \tag{5h}$$

$$\mathbf{u}_{j,\min} \leq \mathbf{u}_j \leq \mathbf{u}_{j,\max} \quad \forall j \in \mathcal{J} \tag{5i}$$

$$a_j \in \{0, 1\} \quad \forall j; \; x_{kj} \in \{0, 1\} \; \forall k, j. \tag{5j}$$

Our goal is to minimize the system cost by jointly optimizing 1) the locations of the UAVs, i.e., $\mathbf{U}$; 2) the fraction of bandwidth, i.e., $\mathbf{F} = [\mathbf{f}_1, \ldots, \mathbf{f}_K]$; 3) the association between the UEs and the UAVs, i.e., $\mathbf{X}$; 4) the transmit power of the UAVs, i.e., $\mathbf{p}$; and 5) the on/off states of UAVs, i.e., $\mathbf{a}$. Here, $C_j(\mathbf{u}_j, \mathbf{a})$ and $R_k(\mathbf{U}, \mathbf{X}, \mathbf{p}, \mathbf{f}_k)$ are given in (2) and (4), respectively.

The objective function (5a) denotes the total system cost, where λ_1 denotes the weight of the UAV deployment cost; (5b) is the required QoS constraint for the UEs; (5c) is the backhaul capacity constraint; (5d) is the transmit power constraint for an active UAV; (5e) shows that each UE can only be served by at most one UAV; (5f) denotes the UAV activation constraint such that the serving UAV must be active; (5g) denotes the constraint for the allocated fraction of bandwidth. (5h) denotes the constraint that only active UAVs can connect to UEs; (5i) is the UAVs' location constraint; and (5j) denotes the binary constraints for a_j and x_{kj}.

Note that, (5) is challenging to be directly solved since the variables are coupled together. Furthermore, (5) involves nonconvex constraints, such as (5b) and (5c), as well as binary variables, such as x_{kj} and a_j. To obtain a solution to this problem, we employ the BCD method [40]. The idea behind the BCD method is to decompose a large optimization problem into several subproblems, which can be easier to solve individually. Specifically, the BCD method first partitions the optimization variables into nonoverlapping blocks and then iteratively solves the optimization problem for one block of variables while keeping the other blocks fixed. This process is repeated until convergence is achieved. For (5), we divide it into two subproblems, namely 1) the subproblem that involves the UAV selection and wireless resource allocation and 2) the subproblem that involves the UAV location. The two subproblems are optimized alternately and iteratively. For each subproblem, we utilize the SCA technique [41] to transform it into a sequence of convex optimization problems. By solving those sequences of convex problems, we obtain a stationary solution for our system cost minimization problem.

B. UAV Selection and Wireless Resource Allocation

For the subproblem that involves the UAV selection and wireless resource allocation, we start with the given UAV locations $\mathbf{U}$ that fulfills (5i), and (5) then degenerates to

$$\min_{\{\mathbf{F},\mathbf{X},\mathbf{p},\mathbf{a}\}} \sum_{j\in\mathcal{J}} p_j + \lambda_1 \sum_{j\in\mathcal{J}} a_j \tag{6a}$$

$$\text{s.t.} \quad R_k(\mathbf{X}, \mathbf{p}, \mathbf{f}_k) \geq \Gamma_k \quad \forall k \in \mathcal{K} \tag{6b}$$

$$\sum_{k\in\mathcal{K}} x_{kj}\Gamma_k \leq C_j(\mathbf{a}) \quad \forall j \in \mathcal{J} \tag{6c}$$

$$(5d)-(5h), (5j). \tag{6d}$$

Then, (6) is still difficult to solve due to the nonconvex constraints (6b) and (6c)[1], as well as the binary variables x_{kj} and a_j.

To handle the nonconvex constraints (6b) and (6c), we introduce the auxiliary variables to transform those constraints into equivalent forms, which facilitates the applications of the

[1]For a convex optimization problem, its objective function must conform to "min convex (or affine) function" or "max concave (or affine) function," and its inequality constraints must conform to "convex (or affine) function $\leq$ concave (or affine) function." Consider degenerated functions $R_k(p) = \log(1+1/(p+1))$ for (6b) and $C_j(a) = \log(2/a-1)$ for (6c), respectively. We can see that $R_k(p)$ is convex and $C_j(a)$ is neither convex nor concave. Therefore, (6b) and (6c) are the nonconvex constraints. Refer to [42] for further details on the convex optimization.

SCA method later. First, the term $\log(1+\mathrm{SINR}_k(\mathbf{X},\mathbf{p}))$ in $R_k(\mathbf{X},\mathbf{p},\mathbf{f}_k)$, which is given by (4), can be written as

$$\log(1+\mathrm{SINR}_k(\mathbf{X},\mathbf{p})) = \log\left(\sum_{j\in\mathcal{J}} p_j G_{kj} + \sigma_k^2\right) - \log\left(\sum_{j\in\mathcal{J}} (1-x_{kj}) p_j G_{kj} + \sigma_k^2\right) \quad \forall k \in \mathcal{K}. \tag{7}$$

For (6b), we introduce the auxiliary variables $\mathbf{r} = \{r_k, k \in \mathcal{K}\}$ and $\mathbf{M} = \{m_{kj}, k \in \mathcal{K}, j \in \mathcal{J}\}$, (6b) can be equivalently transformed to the following ($\forall k \in \mathcal{K}, j \in \mathcal{J}$) using (7):

$$m_{kj} \geq (1-x_{kj}) p_j \tag{8a}$$

$$\log\left(\sum_{j\in\mathcal{J}} p_j G_{kj} + \sigma_k^2\right) - r_k \geq \log\left(\sum_{j\in\mathcal{J}} m_{kj} G_{kj} + \sigma_k^2\right) \tag{8b}$$

$$(1-\beta) B \left(\sum_{j\in\mathcal{J}} f_{kj}\right) r_k \geq \Gamma_k. \tag{8c}$$

To see the equivalence between (8) and (6b), we just plug the expression of m_{kj} in (8a) into (8b) and obtain the expression of r_k. Then, we substitute r_k in (8c) and obtain the inequality (6b).

Moreover, (8a) and (8c) can be equivalently written as ($\forall k \in \mathcal{K}, j \in \mathcal{J}$)

$$4(p_j - m_{kj}) + (x_{kj} - p_j)^2 \leq (x_{kj} + p_j)^2 \tag{9}$$

$$\frac{4\Gamma_k}{(1-\beta)B} + \left(\sum_{j\in\mathcal{J}} f_{kj} - r_k\right)^2 \leq \left(\sum_{j\in\mathcal{J}} f_{kj} + r_k\right)^2. \tag{10}$$

Here, we utilized the equality $4xy = (x+y)^2 - (x-y)^2$.

For (6c), we introduce an auxiliary variable z to transform it equivalently to the following two constraints to handle its nonconvexity:

$$\sum_{j\in\mathcal{J}} a_j \leq \frac{N_\mathrm{T}+1}{z+1} \tag{11a}$$

$$\sum_{k\in\mathcal{K}} x_{kj} \Gamma_k \leq \beta B \log\left(\frac{z P_0 \rho_0}{d_j^{\xi_1} \sigma_j^2 10^{\gamma d_j/10}}\right) \quad \forall j \in \mathcal{J}. \tag{11b}$$

Similar to (8), to see the equivalence between (6c) and (11), we first get the expression of z from (11a). Then, we plug z into (11b) and obtain the inequality (6c).

Furthermore, to deal with the binary variables $\mathbf{X}$ and $\mathbf{a}$, we first relax them to be the continuous variables and introduce a penalty term in the objective function, which enforces the convergence of the continuous variables $\mathbf{X}$ and $\mathbf{a}$ toward the binary values. The penalty term is defined as

$$\mathcal{P}(\mathbf{X},\mathbf{a}) = \lambda_2 \sum_{k\in\mathcal{K}} \sum_{j\in\mathcal{J}} \left(x_{kj} - x_{kj}^2\right) + \lambda_3 \sum_{j\in\mathcal{J}} \left(a_j - a_j^2\right) \tag{12}$$

where λ_2 and λ_3 are the positive penalty factors. Therefore, we can reformulate (6) as

$$\min_{\Omega} \sum_{j\in\mathcal{J}} p_j + \lambda_1 \sum_{j\in\mathcal{J}} a_j + \mathcal{P}(\mathbf{X},\mathbf{a}) \tag{13a}$$

$$\text{s.t.} \quad (5\text{d})-(5\text{h}), (8\text{b}), (9), (10), (11\text{a}), (11\text{b}) \tag{13b}$$

$$0 \leq a_j \leq 1 \quad \forall j; \quad 0 \leq x_{kj} \leq 1 \ \forall k, j. \tag{13c}$$

Here, we denote the set of optimization variables as $\Omega = \{\mathbf{F}, \mathbf{X}, \mathbf{M}, \mathbf{r}, \mathbf{p}, \mathbf{a}, z\}$. Because the right hand side (RHS) of (8b) is a concave function and the RHSs of (9), (10), and (11a) are the convex functions, these constraints do not satisfy the condition for the convex constraints. Hence, (13) is still nonconvex.

Next, we apply the SCA technique to solve (13). The SCA algorithm is an iterative optimization technique to solve the nonconvex optimization problems with specific structures. The main idea behind the SCA algorithm is to iteratively construct a convex approximation of the nonconvex problem around the current point, solve the convex approximation, and then update the point for the next iteration. This process is repeated until convergence or a stopping criterion is met. The convex approximation is done by approximating the nonconvex objective functions and constraints using the appropriate techniques, such as the Taylor series expansion. We first present the following lemma:

Lemma 1 ([42, Sec. 3.1.3]): For a convex differentiable function $f(x)$, $x \in \mathcal{X}$, it can be globally lower bounded by

$$f(x) \geq f\left(x^{(t)}\right) + \nabla f\left(x^{(t)}\right)\left(x - x^{(t)}\right) \quad \forall x \in \mathcal{X} \tag{14}$$

where $x^{(t)}$ is a given point in the domain of f. Moreover, the bound is tight, i.e., $f(x) = f(x^{(t)})$ when $x = x^{(t)}$.

We propose to replace the RHS functions of (8b), (9), (10), and (11a) with their first-order approximations using Lemma 1 as the surrogate functions. The functions $\alpha^{(t)}(\mathbf{m}_k)$, $\chi^{(t)}(x_{kj}, p_j)$,

$$\alpha^{(t)}(\vec{m}_k) \triangleq \log\left(\sum_{j\in\mathcal{J}} m_{kj}^{(t)} G_{kj} + \sigma_k^2\right) + \frac{\sum_{j\in\mathcal{J}} \left(m_{kj} - m_{kj}^{(t)}\right) G_{kj}}{\left(\sum_{j\in\mathcal{J}} m_{kj}^{(t)} G_{kj} + \sigma_k^2\right) \ln 2} \geq \text{RHS of (8b)} \quad \forall k \tag{15}$$

$$\chi^{(t)}(x_{kj}, p_j) \triangleq 2\left(x_{kj}^{(t)} + p_j^{(t)}\right)(x_{kj} + p_j) - \left(x_{kj}^{(t)} + p_j^{(t)}\right)^2 \leq \text{RHS of (9)} \quad \forall k, j \tag{16}$$

$$\vartheta^{(t)}\left(\vec{f}_k, r_k\right) \triangleq 2\left(\sum_{j\in\mathcal{J}} f_{kj}^{(t)} + r_k^{(t)}\right)\left(\sum_{j\in\mathcal{J}} f_{kj} + r_k\right) - \left(\sum_{j\in\mathcal{J}} f_{kj}^{(t)} + r_k^{(t)}\right)^2 \leq \text{RHS of (10)} \quad \forall k, j \tag{17}$$

$$\delta^{(t)}(z) \triangleq (N_\mathrm{T}+1)\left(\frac{1}{z^{(t)}+1} - \frac{z - z^{(t)}}{\left(z^{(t)}+1\right)^2}\right) \leq \text{RHS of (11a)} \tag{18}$$

$\vartheta^{(t)}(\mathbf{f}_k, r_k)$, and $\delta^{(t)}(z)$ in (15), (16), (17), and (18), shown at the bottom of the previous page, are the first-order approximations of the RHS functions of (8b), (9), (10), and (11a) at $\mathbf{m}_k^{(t)}$, $(x_{kj}^{(t)}, p_j^{(t)})$, $(\mathbf{f}_k^{(t)}, r_k^{(t)})$, and $z^{(t)}$, respectively, where $\mathbf{m}_k$ denotes the vector composed of the kth row elements of the matrix $\mathbf{M}$, i.e., $\mathbf{m}_k = [m_{k1}, \ldots, m_{kJ}]^{\mathrm{T}}$. Here, $\{\mathbf{m}_k^{(t)}\}$, $\{x_{kj}^{(t)}\}$, $\{p_j^{(t)}\}$,$\{\mathbf{f}_k^{(t)}\}$, $\{r_k^{(t)}\}$, $z^{(t)}$ are the given values for the corresponding variables in the tth iteration, respectively.

Moreover, the penalty term $\mathcal{P}(\mathbf{X}, \mathbf{a})$ in (13a) is a concave function, whose first-order approximation using Lemma 1 at $\left(x_{kj}^{(t)}, a_j^{(t)}\right)$ can be expressed as

$$\varrho^{(t)}(\mathbf{X}, \mathbf{a}) \triangleq \lambda_2 \sum_{k\in\mathcal{K}} \sum_{j\in\mathcal{J}} \left(\left(x_{kj}^{(t)}\right)^2 + \left(1 - 2x_{kj}^{(t)}\right) x_{kj} \right) + \lambda_3 \sum_{j\in\mathcal{J}} \left(\left(a_j^{(t)}\right)^2 + \left(1 - 2a_j^{(t)}\right) a_j \right) \tag{19}$$

where $\{x_{kj}^{(t)}\}$, $\{a_j^{(t)}\}$ are the values of the corresponding variables in the tth iteration, respectively.

By substituting $\alpha^{(t)}(\mathbf{m}_k)$, $\chi^{(t)}(x_{kj}, p_j)$, $\vartheta^{(t)}(\mathbf{f}_k, r_k)$, $\delta^{(t)}(z)$, and $\varrho^{(t)}(\mathbf{X}, \mathbf{a})$ for the RHS functions of (8b), (9), (10), and (11a) and for the penalty term in (13a), respectively, the objective function become affine and the constraints become convex; (6) can be approximated in the $(t+1)$th iteration as

$$\min_{\Omega} \sum_{j\in\mathcal{J}} p_j + \lambda_1 \sum_{j\in\mathcal{J}} a_j + \varrho^{(t)}(\mathbf{X}, \mathbf{a}) \tag{20a}$$

$$\text{s.t. } (5d)-(5h), (11b), (13c) \tag{20b}$$

$$\log\left(\sum_{j\in\mathcal{J}} p_j G_{kj} + \sigma_k^2 \right) - r_k \geq \alpha^{(t)}(\mathbf{m}_k) \quad \forall k \tag{20c}$$

$$4\left(p_j - m_{kj}\right) + \left(x_{kj} - p_j\right)^2 \leq \chi^{(t)}\left(x_{kj}, p_j\right) \quad \forall k, j \tag{20d}$$

$$\frac{4\Gamma_k}{(1-\beta)B} + \left(\sum_{j\in\mathcal{J}} f_{kj} - r_k \right)^2 \leq \vartheta^{(t)}(\mathbf{f}_k, r_k) \quad \forall k \tag{20e}$$

$$\sum_{j\in\mathcal{J}} a_j \leq \delta^{(t)}(z) \quad \forall j \in \mathcal{J}. \tag{20f}$$

Then, (20) is a convex optimization problem and can be solved using the convex optimization software like CVX [43]. After solving (20), we update the solutions of Ω for the next iteration.

C. UAV Location Optimization

After solving (20) for the UAV selection and wireless resource allocation subproblem, the transmit power of the UAVs $\mathbf{p}$, the on/off states of the UAVs $\mathbf{a}$, the association $\mathbf{X}$ between the UEs and the UAVs, and the fraction of bandwidth $\mathbf{F}$ can be obtained. Then, we fix those values for the corresponding variables and update the UAV locations $\mathbf{U}$. Here, the original problem (5) becomes a feasibility problem with multiple solutions satisfying its feasibility conditions. To facilitate rapid convergence in subsequent iterations, we further transform (5) into a sum rate maximization problem with an explicit objective function. The rationale is that we update the locations of UAVs to achieve the largest increase in the data rates. Consequently, in this location, the required wireless resource consumption of UAVs can be minimized in the next iteration. To this end, we formulate the following problem for updating the UAV locations:

$$\max_{\{\mathbf{U}, \boldsymbol{\phi}\}} \sum_{k\in\mathcal{K}} \phi_k \tag{21a}$$

$$\text{s.t. } R_k(\mathbf{U}) \geq \phi_k \quad \forall k \in \mathcal{K} \tag{21b}$$

$$\phi_k \geq \Gamma_k \quad \forall k \in \mathcal{K} \tag{21c}$$

$$\sum_{k\in\mathcal{K}} x_{kj}\Gamma_k \leq C_j(\mathbf{u}_j) \quad \forall j \in \mathcal{J} \tag{21d}$$

$$(5i). \tag{21e}$$

Here, $\boldsymbol{\phi} = [\phi_1, \ldots, \phi_K]^{\mathrm{T}}$ is the introduced additional variable. Both the UE rate $R_k(\mathbf{U})$ and the backhaul capacity $C_j(\mathbf{u}_j)$ in (21) are determined by the UAV locations, which leads to the nonconvex constraints (21b) and (21d).[2]

To tackle (21b), we rewrite $R_k(\mathbf{U})$ in (21b) as

$$R_k(\mathbf{U}) = (1-\beta)B\left(\sum_{j\in\mathcal{J}} f_{kj} \right) \left(\log\left(\sum_{j\in\mathcal{J}} \frac{p_j \rho_0}{d_{kj}^{\xi_2}} + \sigma_k^2 \right) - \log\left(\sum_{j\in\mathcal{J}} \frac{(1-x_{kj}) p_j \rho_0}{d_{kj}^{\xi_2}} + \sigma_k^2 \right) \right) \quad \forall k \in \mathcal{K}. \tag{22}$$

Then, we introduce the slack variables s_{kj} and v_{kj}, $\forall k \in \mathcal{K}, j \in \mathcal{J}$, and convert (21b) into the following form:

$$d_{kj}^{\xi_2} \leq s_{kj} \quad \forall k \in \mathcal{K}, j \in \mathcal{J} \tag{23a}$$

$$d_{kj}^{\xi_2} \geq v_{kj} \quad \forall k \in \mathcal{K}, j \in \mathcal{J} \tag{23b}$$

$$\phi_k \leq (1-\beta)B\left(\sum_{j\in\mathcal{J}} f_{kj} \right) \theta_k(\mathbf{s}_k, \mathbf{v}_k) \quad \forall k \in \mathcal{K} \tag{23c}$$

where $\mathbf{s}_k = [s_{k1}, \ldots, s_{kJ}]^{\mathrm{T}}$, $\mathbf{v}_k = [v_{k1}, \ldots, v_{kJ}]^{\mathrm{T}}$, and

$$\theta_k(\mathbf{s}_k, \mathbf{v}_k) \triangleq \log\left(\sum_{j\in\mathcal{J}} \frac{p_j \rho_0}{s_{kj}} + \sigma_k^2 \right) - \log\left(\sum_{j\in\mathcal{J}} \frac{(1-x_{kj}) p_j \rho_0}{v_{kj}} + \sigma_k^2 \right) \quad \forall k \in \mathcal{K}. \tag{24}$$

To see the equivalence between (21b) and (23), we just plug the expression of s_{kj} in (23a) and v_{kj} in (23b) into (24) and obtain the expression of $\theta_k(\mathbf{s}_k, \mathbf{v}_k)$. Then, we substitute $\theta_k(\mathbf{s}_k, \mathbf{v}_k)$ in (23c) and obtain the inequality (21b).

Since, the expression of $d_{kj}^{\xi_2}$ on the left-hand-side (LHS) of (23b) is convex with respect to $\mathbf{u}_j$, (23b) is nonconvex. The first-order approximation of $d_{kj}^{\xi_2}$ in (23b) around $\mathbf{u}_j^{(t)}$ using Lemma 1 can be written as $D_{kj}^{(t)}(\mathbf{u}_j)$ in (25), shown at on the bottom of the next page. Here, $\{\mathbf{u}_j^{(t)}\}$ is the given value for

[2]Consider degenerated functions $R_k(u) = \log(1 + (1/u^2)/(1 + 1/u^2))$ and $C_j(u) = \log(1/(u^2 10^{(u/10)}))$. Here, $R_k(u)$ is neither convex nor concave and $C_j(u)$ is convex. Therefore, we see that (21b) and (21d) are the nonconvex constraints.

$\{\mathbf{u}_j\}$ in the tth iteration. Additionally, note that, the first and the second terms of $\theta_k(\mathbf{s}_k, \mathbf{v}_k)$ in (24) are convex with respect to the slack variables $\mathbf{s}_k$ and $\mathbf{v}_k$, respectively. By utilizing Proposition 1, we can obtain a lower bound of $\theta_k(\mathbf{s}_k, \mathbf{v}_k)$ which is a concave function in $(\mathbf{s}_k, \mathbf{v}_k)$

Proposition 1: $\theta_k(\mathbf{s}_k, \mathbf{v}_k)$ is a difference of convex functions and a concave global lower bound of $\theta_k(\mathbf{s}_k, \mathbf{v}_k)$ can be expressed as

$$\theta_k^{(t)}(\mathbf{s}_k, \mathbf{v}_k) \triangleq \log\left(\sum_{j\in\mathcal{J}} \frac{p_j\rho_0}{s_{kj}^{(t)}} + \sigma_k^2\right) - \frac{\sum_{j\in\mathcal{J}} \frac{p_j\rho_0\left(s_{kj}-s_{kj}^{(t)}\right)}{\left(s_{kj}^{(t)}\right)^2 \ln 2}}{\sum_{j\in\mathcal{J}} \frac{p_j\rho_0}{s_{kj}^{(t)}} + \sigma_k^2} - \log\left(\sum_{j\in\mathcal{J}} \frac{(1-x_{kj})p_j\rho_0}{v_{kj}} + \sigma_k^2\right) \tag{26}$$

where $\{s_{kj}^{(t)}\}$ are the given values for $\{s_{kj}\}$ in the tth iteration. The bound is tight at $s_{kj} = s_{kj}^{(t)} \quad \forall k, j$.

Proof: See the Appendix. ∎

To tackle (21d), we observe that the term $-(\xi_1/2)\log(\|\mathbf{u}_j - \mathbf{u}_0\|^2)$ in $C_j(\mathbf{u}_j)$ of (21d) is a convex function with respect to $\|\mathbf{u}_j - \mathbf{u}_0\|^2$. Based on Lemma 1, the first-order Taylor expansion of $C_j(\mathbf{u}_j)$ at $\|\mathbf{u}_j^{(t)} - \mathbf{u}_0\|^2$ can be found as a global lower bound of $C_j(\mathbf{u}_j)$, which is given by $C_j^{(t)}(\mathbf{u}_j)$ in (27), shown at the bottom of the page. Here, $\{\mathbf{u}_j^{(t)}\}$ is the given value for $\{\mathbf{u}_j\}$ in the tth iteration.

We denote $\mathbf{S} = [\mathbf{s}_1, \ldots, \mathbf{s}_K]$ and $\mathbf{V} = [\mathbf{v}_1, \ldots, \mathbf{v}_K]$, and denote the set of optimization variables as $\Phi = \{\mathbf{U}, \mathbf{S}, \mathbf{V}, \boldsymbol{\phi}\}$. By substituting $C_j^{(t)}(\mathbf{u}_j)$ for the RHS function of (21d), $D_{kj}^{(t)}(\mathbf{u}_j)$ and $\theta_k^{(t)}(\mathbf{s}_k, \mathbf{v}_k)$ for the LHS function of (23b), and $\theta_k(\mathbf{s}_k, \mathbf{v}_k)$ in (23c), respectively, (21d), (23b), and (23c) become convex, and (21) can be approximated by the following in the $(t+1)$th iteration:

$$\max_{\Phi} \quad \sum_{k\in\mathcal{K}} \phi_k \tag{28a}$$

$$\text{s.t.} \quad (1-\beta)B\left(\sum_{j\in\mathcal{J}} f_{kj}\right)\theta_k^{(t)}(\mathbf{s}_k, \mathbf{v}_k) \geq \phi_k \quad \forall k \in \mathcal{K} \tag{28b}$$

$$\sum_{k\in\mathcal{K}} x_{kj}\Gamma_k \leq C_j^{(t)}(\mathbf{u}_j) \quad \forall j \in \mathcal{J} \tag{28c}$$

$$D_{kj}^{(t)}(\mathbf{u}_j) \geq v_{kj} \quad \forall k \in \mathcal{K}, j \in \mathcal{J} \tag{28d}$$

$$\text{(5i)}, \ \text{(21c)}, \ \text{(23a)}. \tag{28e}$$

Then, (28) is now convex and can be solved by the convex optimization software like CVX [43]. After solving (28), we update the solutions of Φ for the next iteration.

Algorithm 1 Method for Minimizing System Cost (5)

1: **Initialization:** Initialize $\mathbf{U}^{(0)}$, $\mathbf{S}^{(0)}$, $\mathbf{V}^{(0)}$, $\mathbf{F}^{(0)}$, $\mathbf{X}^{(0)}$, $\mathbf{M}^{(0)}$, $\mathbf{r}^{(0)}$, $\mathbf{p}^{(0)}$, $\mathbf{a}^{(0)}$, $z^{(0)}$ with a feasible point. Set maximum iteration number $I_{\max}$ and set $t = 0$.
2: **repeat**
3: Fix the values of $\mathbf{U}^{(t)}$. Solve problem (20) with the current iteration $\mathbf{F}^{(t)}$, $\mathbf{X}^{(t)}$, $\mathbf{M}^{(t)}$, $\mathbf{r}^{(t)}$, $\mathbf{p}^{(t)}$, $\mathbf{a}^{(t)}$, $z^{(t)}$. Denote its solution as $\mathbf{F}^{(t+1)}$, $\mathbf{X}^{(t+1)}$, $\mathbf{p}^{(t+1)}$, $\mathbf{a}^{(t+1)}$.
4: Fix the values of $\mathbf{F}^{(t+1)}$, $\mathbf{X}^{(t+1)}$, $\mathbf{p}^{(t+1)}$ and $\mathbf{a}^{(t+1)}$. Solve problem (28) with the current iteration $\mathbf{U}^{(t)}$, $\mathbf{S}^{(t)}$, $\mathbf{V}^{(t)}$. Denote its solution as $\mathbf{U}^{(t+1)}$.
5: Update $t = t + 1$
6: **until** convergence criterion is met or $t > I_{\max}$.

D. Overall Algorithm and Convergence

The overall process for solving the system cost minimization problem is shown in Algorithm 1. In Algorithm 1, we use the BCD method to decompose the original optimization problem (5) into the UAV selection and wireless resource allocation subproblem (6), which involves variables $\{\mathbf{F}, \mathbf{X}, \mathbf{p}, \mathbf{a}\}$, and the UAV location optimization subproblem (21), which involves variable $\mathbf{U}$. The two subproblems are still difficult nonconvex optimization problems. Therefore, we first initialize the variables with a feasible point as outlined in Step 1 of Algorithm 1, and then employ the SCA technique to approximate each subproblem using the convex approximations around the current point. At each iteration, we solve the two convex approximated subproblems and update the variables as outlined in Steps 3 and 4 of Algorithm 1, respectively. This process is repeated until the stopping criterion is met.

Starting from a feasible point, Algorithm 1 converges to a stationary point. The convergence of Algorithm 1 is proved in [44]. Specifically, Algorithm 1 decomposes the original problem (5) into two variable blocks, which contains $\{\mathbf{F}, \mathbf{X}, \mathbf{p}, \mathbf{a}\}$, and $\mathbf{U}$, respectively. Then, it updates the variable blocks by successively optimizing a sequence of convex approximations of each subproblem, which are constructed using the tight upper/lower bounds of concave/convex functions. Each iteration solves the approximated subproblems (20) and (28), with the obtained solutions serving as the input for the next iteration. Therefore, Algorithm 1 must converge to a stationary point. Since, the original problem is nonconvex, Algorithm 1 does not guarantee a global optimum solution, but it can find high-quality solutions efficiently.

$$D_{kj}^{(t)}(\mathbf{u}_j) \triangleq \left\|\mathbf{u}_j^{(t)} - \hat{\mathbf{u}}_k\right\|^{\xi_2} + \xi_2\left\|\mathbf{u}_j^{(t)} - \hat{\mathbf{u}}_k\right\|^{\xi_2-2}\left(\mathbf{u}_j^{(t)} - \hat{\mathbf{u}}_k\right)^{\mathrm{T}}\left(\mathbf{u}_j - \mathbf{u}_j^{(t)}\right) \leq \text{LHS of (23b)} \quad \forall k, j \tag{25}$$

$$C_j^{(t)}(\mathbf{u}_j) \triangleq \beta B \log\left(\frac{\left(\frac{N_{\mathrm{T}}+1}{\sum_{j\in\mathcal{J}} a_j} - 1\right)P_0\rho_0}{\sigma_j^2 10^{\gamma(\|\mathbf{u}_j-\mathbf{u}_0\|)/10}}\right) - \frac{\beta B\xi_1}{2}\left(\frac{\|\mathbf{u}_j - \mathbf{u}_0\|^2 - \left\|\mathbf{u}_j^{(t)} - \mathbf{u}_0\right\|^2}{\left\|\mathbf{u}_j^{(t)} - \mathbf{u}_0\right\|^2 \ln 2} + \log\left(\left\|\mathbf{u}_j^{(t)} - \mathbf{u}_0\right\|^2\right)\right) \leq \text{RHS of (21d)} \ \forall j \tag{27}$$

E. Complexity Analysis

Algorithm 1 involves solving the convex problems (20) and (28), where their variable numbers are $3KJ + K + 2J + 1$ and $2KJ + 3K + J$, respectively. By employing a primal-dual interior point method to solve (20) and (28), the computation complexities are, respectively, $\mathcal{O}((3KJ+K+2J+1)^3 \log(\epsilon_1^{-1}))$ and $\mathcal{O}((2KJ + 3K + J)^3 \log(\epsilon_1^{-1}))$ with ϵ_1 being the accepted duality gap [42]. Suppose that, the number of iterations in Algorithm 1 is T_1. Then, the total computation complexity for Algorithm 1 can be calculated as $\mathcal{O}(T_1((3KJ+K+2J+1)^3 + (2KJ + 3K + J)^3) \log(\epsilon_1^{-1}))$.

IV. System Utility Maximization

The system utility in a multi-UAV-assisted wireless network involves the sum rates of the UEs and the UAV deployment costs. We consider the system utility maximization problem in this section and propose its solution.

A. Optimization Problem Formulation

The system utility in a multi-UAV-assisted wireless network is defined as a weighted difference between the sum of the UE data rates and the UAV deployment cost. According to [34], we assume each UAV allocates an equal fraction of bandwidth to its UEs to guarantee fairness for the UEs. Thus, the fraction of bandwidth assigned to the kth UE on the jth UAV can be written as

$$f_{kj} = \begin{cases} 1/b_j, & \text{if } x_{kj} = 1 \\ 0, & \text{if } x_{kj} = 0 \end{cases} \tag{29}$$

where $b_j = \sum_{k\in\mathcal{K}} x_{kj}$ is the variable that indicates the number of UEs served by the jth UAV and we denote $\mathbf{b} = [b_1, \ldots, b_J]^{\mathrm{T}}$.

Further, the SINR of UE k when it is supported by UAV j, i.e., $k \in \mathcal{K}_j$, can be expressed as

$$\mathrm{SINR}_{kj}(\mathbf{U}, \mathbf{p}, \mathbf{b}) = \frac{I_0(b_j) p_j G_{kj}}{\sum_{l\in\mathcal{J}\setminus j} I_0(b_l) p_l G_{kl} + \sigma_k^2} \tag{30}$$

where $I_0(\cdot)$ is an indicator function defined as

$$I_0(b_j) = \begin{cases} 0, & \text{if } b_j = 0 \\ 1, & \text{otherwise.} \end{cases} \tag{31}$$

Using (30), we write $\hat{R}_{kj}(\mathbf{U}, \mathbf{p}, \mathbf{b}) = (1 - \beta)B \log(1 + \mathrm{SINR}_{kj}(\mathbf{U}, \mathbf{p}, \mathbf{b}))$, where $k \in \mathcal{K}_j$.

Now, the system utility maximization problem can be formulated as

$$\max_{\{\mathbf{U},\mathbf{X},\mathbf{p},\bar{\mathbf{r}},\mathbf{b}\}} \sum_{k\in\mathcal{K}} \bar{r}_k - \lambda_4 \sum_{j\in\mathcal{J}} I_0(b_j) \tag{32a}$$

$$\text{s.t.} \quad \sum_{j\in\mathcal{J}} \frac{x_{kj}\hat{R}_{kj}(\mathbf{U}, \mathbf{p}, \mathbf{b})}{b_j} \geq \bar{r}_k \quad \forall k \in \mathcal{K} \tag{32b}$$

$$\sum_{k\in\mathcal{K}} x_{kj}\bar{r}_k \leq C_j(\mathbf{u}_j, \mathbf{b}) \quad \forall j \in \mathcal{J} \tag{32c}$$

$$0 \leq p_j \leq p^{\max} \quad \forall j \in \mathcal{J} \tag{32d}$$

$$\sum_{j\in\mathcal{J}} x_{kj} = 1 \quad \forall k \in \mathcal{K} \tag{32e}$$

$$\mathbf{u}_{j,\min} \leq \mathbf{u}_j \leq \mathbf{u}_{j,\max} \quad \forall j \in \mathcal{J} \tag{32f}$$

$$x_{kj} \in \{0, 1\} \quad \forall k \in \mathcal{K}\ \forall j \in \mathcal{J}. \tag{32g}$$

Here, we introduce the additional variables $\bar{r}_k$ for the data rate of UE k and denote $\bar{\mathbf{r}} = [\bar{r}_1, \ldots, \bar{r}_K]^{\mathrm{T}}$. Moreover, we replace the number of active UAVs $\sum_{j\in\mathcal{J}} a_j$ with $\sum_{j\in\mathcal{J}} I_0(b_j)$ in $C_j(\mathbf{u}_j, \mathbf{a})$ of (2) and rewrite it as $C_j(\mathbf{u}_j, \mathbf{b})$ in (32).

The objective function (32a) denotes the system utility, λ_4 denotes the weight of the UAV, the deployment cost (32b) is the expression for the UE data rate, (32c) is the backhaul capacity constraint, (32d) is the transmit power constraint for an active UAV, (32e) shows that each UE can only be served by at most one UAV, (32f) is the UAVs' location constraint, and (32g) denotes the binary constraint from the definitions.

Note that, (32) is difficult to solve since the variables are coupled together. Furthermore, (32) involves the nonconvex constraints, such as (32b) and (32c) as well as the binary variable x_{kj}. In the following, we address (32) using the BCD method combined with SCA that alternately solves the following two subproblems: 1) the subproblem that involves the UAV selection and wireless resource allocation, and 2) the subproblem that involves the UAV location optimization.

B. UAV Selection and Wireless Resource Allocation

For the subproblem that involves the UAV selection and wireless resource allocation, we start with the given UAV locations $\mathbf{U}$ that fills (32f), and (32) then degenerates to

$$\max_{\{\mathbf{X},\mathbf{p},\bar{\mathbf{r}},\mathbf{b}\}} \sum_{k\in\mathcal{K}} \bar{r}_k - \lambda_4 \sum_{j\in\mathcal{J}} I_0(b_j) \tag{33a}$$

$$\text{s.t.} \quad \sum_{j\in\mathcal{J}} \frac{x_{kj}\hat{R}_{kj}(\mathbf{p}, \mathbf{b})}{b_j} \geq \bar{r}_k \ \forall k \in \mathcal{K} \tag{33b}$$

$$\sum_{k\in\mathcal{K}} x_{kj}\bar{r}_k \leq C_j(\mathbf{b}) \quad \forall j \in \mathcal{J} \tag{33c}$$

$$(32d), (32e), (32g). \tag{33d}$$

Then, (33) is still difficult to solve because it involves the nonconvex constraints (33b) and (33c),[3] Nonsmooth functions $I_0(\cdot)$, as well as the binary variables x_{kj}. To handle the nonconvex constraints (33b) and (33c), we introduce auxiliary variables to transform those constraints into equivalent forms, which facilitates the applications of the SCA method later.

For (33b), from the assumption that UE k is associated with only one UAV according to (32e), we can rewrite constraint (33b) as

$$x_{kj}\left(\hat{R}_{kj}(\mathbf{p}, \mathbf{b}) - \bar{r}_k b_j\right) \geq 0 \quad \forall k \in \mathcal{K}, j \in \mathcal{J}. \tag{34}$$

Further, we rewrite $\hat{R}_{kj}(\mathbf{p}, \mathbf{b})$ as

$$\hat{R}_{kj}(\mathbf{p}, \mathbf{b}) = (1 - \beta)B\left(\log\left(\sum_{j\in\mathcal{J}} I_0(b_j) p_j G_{kj} + \sigma_k^2\right) - \log\left(\sum_{l\in\mathcal{J}\setminus j} I_0(b_l) p_l G_{kl} + \sigma_k^2\right)\right) \quad \forall k \in \mathcal{K}, j \in \mathcal{J} \tag{35}$$

[3]To see that (33b) and (33c) are nonconvex constraints, we can follow similar discussions as those for (6).

and introduce the auxiliary variables $\mathbf{h} = [h_1, \ldots, h_J]^{\mathrm{T}}$, $\mathbf{g} = [g_1, \ldots, g_J]^{\mathrm{T}}$, $\mathbf{q} = [q_1, \ldots, q_J]^{\mathrm{T}}$, $\mathbf{e} = [e_1, \ldots, e_J]^{\mathrm{T}}$, and $K \times J$ matrices $\boldsymbol{\Upsilon}$ and $\mathbf{W}$ whose (k, j)th elements are Υ_{kj} and w_{kj}, respectively. Then, we can equivalently transform (34) to the following ($\forall k \in \mathcal{K}, j \in \mathcal{J}$) using (35):

$$I_0(b_j) \geq h_j \tag{36a}$$
$$I_0(b_j) \leq g_j \tag{36b}$$
$$h_j p_j \geq q_j \tag{36c}$$
$$g_j p_j \leq e_j \tag{36d}$$
$$\Upsilon_{kj} + \log\left(\sum_{l \in \mathcal{J} \setminus j} e_l G_{kl} + \sigma_k^2\right) \leq \log\left(\sum_{j \in \mathcal{J}} q_j G_{kj} + \sigma_k^2\right) \tag{36e}$$
$$(1-\beta) B \Upsilon_{kj} - \bar{r}_k b_j \geq w_{kj} \tag{36f}$$
$$x_{kj} w_{kj} \geq 0. \tag{36g}$$

To see the equivalence between (34) and (36), we just plug the expression of q_j in (36c) and e_j in (36d) into (36e) and obtain the expression of Υ_{kj}. Then, we substitute Υ_{kj} in (36f) and obtain the expression of w_{kj}. After that, we substitute w_{kj} in (36g) and obtain the inequality (34).

To tackle the nonsmooth function $I_0(\cdot)$, we approximate the term $I_0(b_j)$ on the LHS of (36a) and (36b) as follows according to [45]:

$$I_0(b_j) \approx \frac{\log\left(1 + \epsilon^{-1} b_j\right)}{\log\left(1 + \epsilon^{-1}\right)} \quad \forall j \in \mathcal{J} \tag{37}$$

where ϵ is a small constant.

To tackle the nonconvex constraint (33c), we introduce an auxiliary variable $\bar{z}$ and transform it equivalently to the following two constraints:

$$\sum_{j \in \mathcal{J}} I_0(b_j) \leq \frac{N_{\mathrm{T}} + 1}{\bar{z} + 1} \tag{38a}$$
$$\sum_{k \in \mathcal{K}} x_{kj} \bar{r}_k \leq \beta B \log\left(\frac{\bar{z} P_0 \rho_0}{d_j^{\xi_1} \sigma_j^2 10^{\gamma d_j / 10}}\right) \quad \forall j \in \mathcal{J}. \tag{38b}$$

The equivalence between (33c) and (38) can be obtained by the first getting expression of $\bar{z}$ from (38a) and then substituting the expression of $\bar{z}$ into (38b).

Moreover, (36c), (36d), (36f), (36g), and (38b) can be equivalently written as ($\forall k \in \mathcal{K}, j \in \mathcal{J}$)

$$\frac{1}{4}(h_j + p_j)^2 \geq \frac{1}{4}(h_j - p_j)^2 + q_j \tag{39}$$
$$\frac{1}{4}(g_j + p_j)^2 \leq \frac{1}{4}(g_j - p_j)^2 + e_j \tag{40}$$
$$(1-\beta) B \Upsilon_{kj} + \frac{1}{4}(\bar{r}_k - b_j)^2 \geq \frac{1}{4}(\bar{r}_k + b_j)^2 + w_{kj} \tag{41}$$
$$\frac{1}{4}(x_{kj} + w_{kj})^2 \geq \frac{1}{4}(x_{kj} - w_{kj})^2 \tag{42}$$
$$\sum_{k \in \mathcal{K}} \frac{1}{4}(x_{kj} + \bar{r}_k)^2 \leq \sum_{k \in \mathcal{K}} \frac{1}{4}(x_{kj} - \bar{r}_k)^2 + \log\left(\frac{\bar{z} P_0 \rho_0}{d_j^{\xi_1} \sigma_j^2 10^{\gamma d_j / 10}}\right). \tag{43}$$

Here, we utilized the equality $4xy = (x + y)^2 - (x - y)^2$.

Therefore, by relaxing $\mathbf{X}$ to be continuous variables, we can reformulate (33) as

$$\max_{\Pi} \sum_{k \in \mathcal{K}} \bar{r}_k - \lambda_4 \sum_{j \in \mathcal{J}} \frac{\log\left(1 + \epsilon^{-1} b_j\right)}{\log\left(1 + \epsilon^{-1}\right)} \tag{44a}$$
$$\text{s.t. } 0 \leq x_{kj} \leq 1 \quad \forall k \in \mathcal{K}, j \in \mathcal{J} \tag{44b}$$
$$(32d),\ (32e),\ (36a),\ (36b),\ (36e) \tag{44c}$$
$$(38a),\ (39)\text{–}(43). \tag{44d}$$

Here, we denote the set of optimization variables as $\Pi \triangleq \{\mathbf{X}, \mathbf{W}, \boldsymbol{\Upsilon}, \mathbf{h}, \mathbf{g}, \mathbf{q}, \mathbf{e}, \mathbf{p}, \bar{\mathbf{r}}, \mathbf{b}, \bar{z}\}$ because the LHSs of (36b), (36e), and (38a) are the concave functions, the LHSs of (39), (41), and (42) and the RHSs of (38a) and (40) are the convex functions, and the RHS of (43) is a sum of the convex and concave functions, and (44) is still nonconvex.

Next, we apply the SCA technique to solve (44). We propose to replace the LHS functions of (36b), (36e), (38a), (39), (41), and (42), the RHS functions of (38a) and (40), and the first term on the RHS of (43) with their first-order approximations using Lemma 1 around $b_j^{(t)}$, $\mathbf{e}^{(t)}$, $\mathbf{b}^{(t)}$, $(h_j^{(t)}, p_j^{(t)})$, $(\bar{r}_k^{(t)}, b_j^{(t)})$, $(x_{kj}^{(t)}, w_{kj}^{(t)})$, $\bar{z}^{(t)}$, $(g_j^{(t)}, p_j^{(t)})$, and $(\mathbf{x}_j^{(t)}, \bar{\mathbf{r}}^{(t)})$ as the surrogate functions, which are denoted as $\varphi^{(t)}(b_j)$, $\tau^{(t)}(\Upsilon_{kj}, \mathbf{e})$, $\kappa^{(t)}(\mathbf{b})$, $\varsigma^{(t)}(h_j, p_j)$, $\zeta^{(t)}(\Upsilon_{kj}, \bar{r}_k, b_j)$, $\varpi^{(t)}(x_{kj}, w_{kj})$, $\iota^{(t)}(\bar{z})$, $\varkappa^{(t)}(g_j, p_j, e_j)$, and $\psi^{(t)}(\mathbf{x}_j, \bar{\mathbf{r}})$ in (45)–(53), shown at the bottom of the next page, respectively, where $\mathbf{x}_j$ denotes the jth column of matrix $\mathbf{X}$, i.e., $\mathbf{x}_j = [x_{1j}, \ldots, x_{Kj}]^{\mathrm{T}}$. Here, $\{b_j^{(t)}\}$, $\mathbf{e}^{(t)}$, $\bar{z}^{(t)}$, $\mathbf{b}^{(t)}$, $\{h_j^{(t)}\}$, $\{g_j^{(t)}\}$, $\{p_j^{(t)}\}$, $\{\bar{r}_k^{(t)}\}$, $\{x_{kj}^{(t)}\}$, $\{w_{kj}^{(t)}\}$, $\{\mathbf{x}_j^{(t)}\}$, and $\bar{\mathbf{r}}^{(t)}$ are the given values for the corresponding variables in the tth iteration.

Furthermore, the objective function in (44a) is convex. Thus, we propose to use its first-order approximation as the surrogate function according to Lemma 1, which can be expressed as $\mathcal{U}_{\mathrm{sys}}^{\mathrm{lb}}(\bar{\mathbf{r}}, \mathbf{b}) = \sum_{k \in \mathcal{K}} \bar{r}_k - \lambda_4 \kappa^{(t)}(\mathbf{b})$. By substituting $\varphi^{(t)}(b_j)$, $\tau^{(t)}(\Upsilon_{kj}, \mathbf{e})$, $\kappa^{(t)}(\mathbf{b})$, $\varsigma^{(t)}(h_j, p_j)$, $\zeta^{(t)}(\Upsilon_{kj}, \bar{r}_k, b_j)$, and $\varpi^{(t)}(x_{kj}, w_{kj})$ for the LHS functions of (36b), (36e), (38a), (39), (41), and (42), respectively, $\iota^{(t)}(\bar{z})$, $\varkappa^{(t)}(g_j, p_j, e_j)$, and $\psi^{(t)}(\mathbf{x}_j, \bar{\mathbf{r}})$ for the RHS functions of (38a), (40), and (43), respectively, the objective function becomes affine and the constraints become convex; (44) can be approximated in the $(t+1)$th iteration as follows:

$$\max_{\Pi} \ \mathcal{U}_{\mathrm{sys}}^{\mathrm{lb}}(\bar{\mathbf{r}}, \mathbf{b}) \tag{54a}$$
$$\text{s.t. } \varphi^{(t)}(b_j) \leq g_j \quad \forall j \tag{54b}$$
$$\tau^{(t)}(\Upsilon_{kj}, \mathbf{e}) \leq \log\left(\sum_{j \in \mathcal{J}} q_j G_{kj} + \sigma_k^2\right) \quad \forall k, j \tag{54c}$$
$$\kappa^{(t)}(\mathbf{b}) \leq \iota^{(t)}(\bar{z}) \quad \forall j \tag{54d}$$
$$\varsigma^{(t)}(h_j, p_j) \geq \frac{1}{4}(h_j - p_j)^2 + q_j \quad \forall j \tag{54e}$$
$$\frac{1}{4}(g_j + p_j)^2 \leq \varkappa^{(t)}(g_j, p_j, e_j) \quad \forall j \tag{54f}$$
$$\zeta^{(t)}(\Upsilon_{kj}, \bar{r}_k, b_j) \geq \frac{1}{4}(\bar{r}_k + b_j)^2 + w_{kj} \quad \forall k, j \tag{54g}$$
$$\varpi^{(t)}(x_{kj}, w_{kj}) \geq \frac{1}{4}(x_{kj} - w_{kj})^2 \quad \forall k, j \tag{54h}$$

$$\sum_{k\in\mathcal{K}}\frac{1}{4}\left(x_{kj}+\bar{r}_k\right)^2 \le \psi^{(t)}\left(\mathbf{x}_j,\bar{\mathbf{r}}\right)+\log\left(\frac{\bar{z}P_0\rho_0}{d_j^{\xi_1}\sigma_j^2 10^{\gamma d_j/10}}\right) \quad \forall k,j \tag{54i}$$

(32d), (32e), (36a), (44b). (54j)

Problem (54) is now a convex optimization problem, and it can be solved by the toolbox CVX [43]. After solving (54), we update the solutions of Π for the next iteration.

C. UAV Location Optimization

After solving (54) for the UAV selection and wireless resource allocation subproblem, we obtain the transmit power $\mathbf{p}$ of the UAVs and the association matrix $\mathbf{X}$ between the UAVs and the UEs. Then, we fix those values for the corresponding variables and update the UAV locations $\mathbf{U}$. At this time, the original problem (32) becomes

$$\max_{\{\mathbf{U},\bar{\mathbf{r}}\}} \quad \sum_{k\in\mathcal{K}}\bar{r}_k-\lambda_4\sum_{j\in\mathcal{J}}I_0(b_j) \tag{55a}$$

$$\text{s.t.} \quad \sum_{j\in\mathcal{J}}\frac{x_{kj}\hat{R}_{kj}(\mathbf{U})}{b_j}\ge\bar{r}_k \quad \forall k\in\mathcal{K} \tag{55b}$$

$$\sum_{k\in\mathcal{K}}x_{kj}\bar{r}_k\le C_j(\mathbf{u}_j) \quad \forall j\in\mathcal{J} \tag{55c}$$

(32f). (55d)

Both the UE rate $\hat{R}_{kj}(\mathbf{U})$ and the backhaul capacity $C_j(\mathbf{u}_j)$ are determined by the UAV locations, which leads to the nonconvex constraints in (55b) and (55c).

To tackle (55b), we rewrite $\hat{R}_{kj}(\mathbf{U})$ in (55b) as

$$\hat{R}_{kj}(\mathbf{U})=(1-\beta)B\left(\log\left(\sum_{j\in\mathcal{J}}\frac{I_0(b_j)p_j\rho_0}{d_{kj}^{\xi_2}}+\sigma_k^2\right)-\log\left(\sum_{l\in\mathcal{J}\setminus j}\frac{I_0(b_l)p_l\rho_0}{d_{kl}^{\xi_2}}+\sigma_k^2\right)\right) \quad \forall k\in\mathcal{K}. \tag{56}$$

Then, we introduce the slack variables $\bar{s}_{kj}$ and $\bar{v}_{kj}$ $\forall j\in\mathcal{J},k\in\mathcal{K}$, to convert (55b) into the following form:

$$d_{kj}^{\xi_2}\le\bar{s}_{kj} \quad \forall k\in\mathcal{K},j\in\mathcal{J} \tag{57a}$$

$$d_{kj}^{\xi_2}\ge\bar{v}_{kj} \quad \forall k\in\mathcal{K},j\in\mathcal{J} \tag{57b}$$

$$\bar{r}_k\le(1-\beta)B\sum_{j\in\mathcal{J}}\frac{x_{kj}\eta_{kj}(\bar{\mathbf{s}}_k,\bar{\mathbf{v}}_k)}{b_j} \quad \forall k\in\mathcal{K} \tag{57c}$$

where $\bar{\mathbf{s}}_k=[\bar{s}_{k1},\ldots,\bar{s}_{kJ}]^{\mathrm{T}}$, $\bar{\mathbf{v}}_k=[\bar{v}_{k1},\ldots,\bar{v}_{kJ}]^{\mathrm{T}}$, and

$$\eta_{kj}(\bar{\mathbf{s}}_k,\bar{\mathbf{v}}_k)\triangleq\log\left(\sum_{j\in\mathcal{J}}\frac{I_0(b_j)p_j\rho_0}{\bar{s}_{kj}}+\sigma_k^2\right)-\log\left(\sum_{l\in\mathcal{J}\setminus j}\frac{I_0(b_l)p_l\rho_0}{\bar{v}_{kl}}+\sigma_k^2\right) \quad \forall k\in\mathcal{K}. \tag{58}$$

To see the equivalence between (55b) and (57), we just plug the expression of $\bar{s}_{kj}$ in (57a) and $\bar{v}_{kj}$ in (57b) into (58) and obtain the expression of $\eta_{kj}(\bar{\mathbf{s}}_k,\bar{\mathbf{v}}_k)$. Then, we substitute $\eta_{kj}(\bar{\mathbf{s}}_k,\bar{\mathbf{v}}_k)$ in (57c) and obtain the inequality (55b).

Since, the expression of $d_{kj}^{\xi_2}$ in (57b) is convex with respect to $\mathbf{u}_j$, (57b) is nonconvex. The first-order approximations of $d_{kj}^{\xi_2}$

$$\varphi^{(t)}(b_j)\triangleq\frac{1}{\log\left(1+\epsilon^{-1}\right)}\left(\log\left(1+\epsilon^{-1}b_j^{(t)}\right)+\frac{b_j-b_j^{(t)}}{\left(\epsilon+b_j^{(t)}\right)\ln 2}\right)\ge\text{LHS of (36b)} \quad \forall j \tag{45}$$

$$\tau^{(t)}\left(\Upsilon_{kj},\vec{e}\right)\triangleq\Upsilon_{kj}+\log\left(\sum_{l\in\mathcal{J}\setminus j}e_l^{(t)}G_{kl}+\sigma_k^2\right)+\frac{\sum_{l\in\mathcal{J}\setminus j}G_{kl}\left(e_l-e_l^{(t)}\right)}{\left(\sum_{l\in\mathcal{J}\setminus j}e_l^{(t)}G_{kl}+\sigma_k^2\right)\ln 2}\ge\text{LHS of (36e)} \quad \forall k,j \tag{46}$$

$$\kappa^{(t)}(\vec{b})\triangleq\frac{1}{\log\left(1+\epsilon^{-1}\right)}\sum_{j\in\mathcal{J}}\left(\log\left(1+\epsilon^{-1}b_j^{(t)}\right)+\frac{b_j-b_j^{(t)}}{\left(\epsilon+b_j^{(t)}\right)\ln 2}\right)\ge\text{LHS of (38a)} \quad \forall j \tag{47}$$

$$\varsigma^{(t)}(h_j,p_j)\triangleq\frac{1}{4}\left(2\left(h_j^{(t)}+p_j^{(t)}\right)\left(h_j+p_j\right)-\left(h_j^{(t)}+p_j^{(t)}\right)^2\right)\le\text{LHS of (39)} \quad \forall j \tag{48}$$

$$\zeta^{(t)}\left(\Upsilon_{kj},\bar{r}_k,b_j\right)\triangleq(1-\beta)B\Upsilon_{kj}+\frac{1}{4}\left(2\left(\bar{r}_k^{(t)}-b_j^{(t)}\right)\left(\bar{r}_k-b_j\right)-\left(\bar{r}_k^{(t)}-b_j^{(t)}\right)^2\right)\le\text{LHS of (41)} \quad \forall k,j \tag{49}$$

$$\varpi^{(t)}(x_{kj},w_{kj})\triangleq\frac{1}{4}\left(2\left(x_{kj}^{(t)}+w_{kj}^{(t)}\right)\left(x_{kj}+w_{kj}\right)-\left(x_{kj}^{(t)}+w_{kj}^{(t)}\right)^2\right)\le\text{LHS of (42)} \quad \forall k,j. \tag{50}$$

$$\iota^{(t)}(\bar{z})\triangleq(N_{\mathrm{T}}+1)\left(\frac{1}{\bar{z}^{(t)}+1}-\frac{\bar{z}-\bar{z}^{(t)}}{\left(\bar{z}^{(t)}+1\right)^2}\right)\le\text{RHS of (36b)} \tag{51}$$

$$\varkappa^{(t)}(g_j,p_j,e_j)\triangleq\frac{1}{4}\left(2\left(g_j^{(t)}-p_j^{(t)}\right)\left(g_j-p_j\right)-\left(g_j^{(t)}-p_j^{(t)}\right)^2\right)+e_j\le\text{RHS of (40)} \quad \forall j \tag{52}$$

$$\psi^{(t)}\left(\vec{x}_j,\bar{\vec{r}}\right)\triangleq\sum_{k\in\mathcal{K}}\frac{1}{4}\left(2\left(x_{kj}^{(t)}-\bar{r}_k^{(t)}\right)\left(x_{kj}-\bar{r}_k\right)-\left(x_{kj}^{(t)}-\bar{r}_k^{(t)}\right)^2\right)\le\text{First term of RHS of (43)} \quad \forall k,j \tag{53}$$

in (57b) around $\mathbf{u}_j^{(t)}$ using Lemma 1 can be written as $\bar{D}_{kj}^{(t)}(\mathbf{u}_j)$ in (59), shown at the bottom of the page. Here, $\{\mathbf{u}_j^{(t)}\}$ is the given value for $\{\mathbf{u}_j\}$ in the tth iteration. Additionally, note that the first and the second terms of $\eta_{kj}(\bar{\mathbf{s}}_k, \bar{\mathbf{v}}_k)$ are convex with respect to slack variables $\bar{\mathbf{s}}_k$ and $\bar{\mathbf{v}}_k$, respectively. By utilizing Proposition 2, we can obtain a lower bound of $\eta_{kj}(\bar{\mathbf{s}}_k, \bar{\mathbf{v}}_k)$ which is a concave function in $(\bar{\mathbf{s}}_k, \bar{\mathbf{v}}_k)$.

Proposition 2: $\eta_{kj}(\bar{\mathbf{s}}_k, \bar{\mathbf{v}}_k)$ is a difference of convex functions and a concave global lower bound of $\eta_{kj}(\bar{\mathbf{s}}_k, \bar{\mathbf{v}}_k)$ can be expressed as

$$\eta_{kj}^{(t)}(\bar{\mathbf{s}}_k, \bar{\mathbf{v}}_k) \triangleq \log\left(\sum_{j\in\mathcal{J}} \frac{I_0(b_j)p_j\rho_0}{\bar{s}_{kj}^{(t)}} + \sigma_k^2\right) - \frac{\sum_{j\in\mathcal{J}} \frac{I_0(b_j)p_j\rho_0\left(\bar{s}_{kj}-\bar{s}_{kj}^{(t)}\right)}{\left(\bar{s}_{kj}^{(t)}\right)^2 \ln 2}}{\sum_{j\in\mathcal{J}} \frac{I_0(b_j)p_j\rho_0}{\bar{s}_{kj}^{(t)}} + \sigma_k^2} - \log\left(\sum_{l\in\mathcal{J}\setminus j} \frac{I_0(b_l)p_l\rho_0}{\bar{v}_{kl}} + \sigma_k^2\right) \tag{60}$$

where $\{\bar{s}_{kj}^{(t)}\}$ are the given values for $\{\bar{s}_{kj}\}$ in the tth iteration. The bound is tight at $\bar{s}_{kj} = \bar{s}_{kj}^{(t)} \quad \forall k, j$.

Proof: See the Appendix. ∎

To tackle (55c), we observed that the term $-(\xi_1/2)\log(\|\mathbf{u}_j - \mathbf{u}_0\|^2)$ in $C_j(\mathbf{u}_j)$ of (55c) is a convex function with respect to $\|\mathbf{u}_j - \mathbf{u}_0\|^2$. Based on Lemma 1, the first-order Taylor expansion of $C_j(\mathbf{u}_j)$ at $\|\mathbf{u}_j^{(t)} - \mathbf{u}_0\|^2$ can be found as a global lower bound of $C_j(\mathbf{u}_j)$, which is given by $\bar{C}_j^{(t)}(\mathbf{u}_j)$ in (61), shown at the bottom of the page. Here, $\{\mathbf{u}_j^{(t)}\}$ is the given value for $\{\mathbf{u}_j\}$ in the tth iteration.

We denote $\bar{\mathbf{S}} = [\bar{\mathbf{s}}_1, \ldots, \bar{\mathbf{s}}_K]$ and $\bar{\mathbf{V}} = [\bar{\mathbf{v}}_1, \ldots, \bar{\mathbf{v}}_K]$, and denote the set of optimization variables as $\beth \triangleq \{\mathbf{U}, \bar{\mathbf{S}}, \bar{\mathbf{V}}, \bar{\mathbf{r}}\}$. By substituting $\bar{C}_j^{(t)}(\mathbf{u}_j)$ for the RHS of (55c), $\bar{D}_{kj}^{(t)}(\mathbf{u}_j)$ and $\eta_{kj}^{(t)}(\bar{\mathbf{s}}_k, \bar{\mathbf{v}}_k)$ for the LHS of (57b) and $\eta_{kj}(\bar{\mathbf{s}}_k, \bar{\mathbf{v}}_k)$ in (57c), respectively, (55c), (57b), and (57c) become convex, and (55) can be approximated as follows in the $(t+1)$th iteration:

$$\max_{\beth} \quad \sum_{k\in\mathcal{K}} \bar{r}_k - \lambda_4 \sum_{j\in\mathcal{J}} I_0(b_j) \tag{62a}$$

$$\text{s.t.} \quad (1-\beta)B \sum_{j\in\mathcal{J}} \frac{x_{kj}\eta_{kj}^{(t)}(\bar{\mathbf{s}}_k, \bar{\mathbf{v}}_k)}{b_j} \geq \bar{r}_k \quad \forall k \in \mathcal{K} \tag{62b}$$

$$\sum_{k\in\mathcal{K}} x_{kj}\bar{r}_k \leq \bar{C}_j^{(t)}(\mathbf{u}_j) \quad \forall j \in \mathcal{J} \tag{62c}$$

$$\bar{D}_{kj}^{(t)}(\mathbf{u}_j) \geq \bar{v}_{kj} \quad \forall k \in \mathcal{K}, j \in \mathcal{J} \tag{62d}$$

$$(32f), (57a). \tag{62e}$$

Algorithm 2 Method for Maximizing System Utility (32)

1: **Initialization:** Initialize $\mathbf{U}^{(0)}$, $\bar{\mathbf{S}}^{(0)}$, $\bar{\mathbf{V}}^{(0)}$, $\mathbf{X}^{(0)}$, $\mathbf{W}^{(0)}$, $\mathbf{p}^{(0)}$, $\mathbf{b}^{(0)}$, $\mathbf{h}^{(0)}$, $\mathbf{g}^{(0)}$, $\mathbf{e}^{(0)}$, $\bar{\mathbf{r}}^{(0)}$, $\bar{z}^{(0)}$ with a feasible point. Set maximum iteriation number $I_{\max}$and set $t = 0$.
2: **repeat**
3: Fix the values of $\mathbf{U}^{(t)}$. Solve problem (54) with the current iteration $\mathbf{X}^{(t)}$, $\mathbf{W}^{(t)}$, $\mathbf{p}^{(t)}$, $\mathbf{b}^{(t)}$, $\mathbf{h}^{(t)}$, $\mathbf{g}^{(t)}$, $\mathbf{e}^{(t)}$, $\bar{\mathbf{r}}^{(t)}$ and $\bar{z}^{(t)}$. Denote its solution as $\mathbf{p}^{(t+1)}$, $\mathbf{X}^{(t+1)}$ and $\mathbf{b}^{(t+1)}$.
4: Fix the values of $\mathbf{p}^{(t+1)}$, $\mathbf{X}^{(t+1)}$ and $\mathbf{b}^{(t+1)}$. Solve problem (62) with the current iteration $\mathbf{U}^{(t)}$, $\bar{\mathbf{S}}^{(t)}$, $\bar{\mathbf{V}}^{(t)}$. Denote its solution as $\mathbf{U}^{(t+1)}$.
5: Update $t = t + 1$
6: **until** convergence criterion is met or $t \geq I_{\max}$

Then, (62) is a convex optimization problem and can be efficiently solved by the CVX toolbox. After solving (62), we update the solutions of $\beth$ for the next iteration.

D. Overall Algorithm and Convergence

The overall process for solving the system utility maximization problem is shown in Algorithm 2. In Algorithm 2, we use the BCD method to decompose the original optimization problem (32) into the UAV selection and wireless resource allocation subproblem (54), which involves variables $\{\mathbf{U}, \mathbf{X}, \mathbf{p}, \bar{\mathbf{r}}, \mathbf{b}\}$, and the UAV location optimization subproblem (62), which involves the variable $\mathbf{U}$. The two subproblems are still difficult nonconvex optimization problems. Therefore, we first initialize the variables with a feasible point as outlined in Step 1 of Algorithm 2 and then employ the SCA technique to approximate each subproblem using the convex approximations around the current point. At each iteration, we solve the two convex approximated subproblems and update the variables as outlined in Steps 3 and 4 of Algorithm 2, respectively. This process is repeated until the stopping criterion is met.

Following the same analysis as Algorithm 1 in Section III-D, starting from a feasible point, Algorithm 2 must converge to a stationary point.

E. Complexity Analysis

Following similar analysis as Algorithm 1 in Section III-E, the overall complexity of Algorithm 2 can be expressed as $\mathcal{O}(T_2(3KJ+K+6J+1)^3 + (2KJ+K+3J)^3)\log(\epsilon_1^{-1}))$ with ϵ_1 being the accepted duality gap [42], where T_2 is the number of iterations in Algorithm 2.

$$\bar{D}_{kj}^{(t)}(\mathbf{u}_j) \triangleq \left\|\mathbf{u}_j^{(t)} - \hat{\mathbf{u}}_k\right\|^{\xi_2} + \xi_2\left\|\mathbf{u}_j^{(t)} - \hat{\mathbf{u}}_k\right\|^{\xi_2-2}\left(\mathbf{u}_j^{(t)} - \hat{\mathbf{u}}_k\right)^{\mathrm{T}}\left(\mathbf{u}_j - \mathbf{u}_j^{(t)}\right) \leq \text{LHS of (57b)} \quad \forall k, j \tag{59}$$

$$\bar{C}_j^{(t)}(\mathbf{u}_j) \triangleq \beta B \log\left(\frac{\left(\frac{N_{\mathrm{T}}+1}{\sum_{j\in\mathcal{J}} I_0(b_j)} - 1\right)P_0\rho_0}{\sigma_j^2 10^{\gamma(\|\mathbf{u}_j-\mathbf{u}_0\|)/10}}\right) - \frac{\beta B\xi_1}{2}\left(\frac{\|\mathbf{u}_j - \mathbf{u}_0\|^2 - \left\|\mathbf{u}_j^{(t)} - \mathbf{u}_0\right\|^2}{\left\|\mathbf{u}_j^{(t)} - \mathbf{u}_0\right\|^2 \ln 2} + \log\left(\left\|\mathbf{u}_j^{(t)} - \mathbf{u}_0\right\|^2\right)\right) \leq \text{RHS of (55c)} \ \forall j. \tag{61}$$

TABLE II
SIMULATION PARAMETERS

Symbols	Value	Physical Meaning
B	1 MHz	System total bandwidth
ρ_0	10^{-3}	Channel power gain
ϵ	10^{-6}	Constant in (37)
z_0	30 m	Altitude of GBS
N_{T}	64	GBS antenna array size
σ_j^2	-102 dBm	Gaussian noise power at the jth UAV
σ_k^2	-102 dBm	Gaussian noise power at the kth UE
ξ_1	3	Pathloss coefficient for backhaul links
ξ_2	3	Pathloss coefficient for access links
P_0	5 W	GBS transmit power
$u^z_{j,\max}$, $u^z_{j,\min}$	200 m, 35 m	Maximum/Minimum altitude of UAV
$p^{\max}$	1 W	Maximum transmit power of UAV
β	0.5	Bandwidth allocation coefficient

V. SIMULATION RESULT

In this section, numerical simulations are conducted to evaluate Algorithms 1 and 2 for the system cost minimization and the system utility maximization problems under the parameters listed in Table II. For performance comparison, we use the following schemes as benchmark methods.

1) *Random-Greedy:* We randomly generate aerial locations for the UAVs following an uniform distribution and use a greedy algorithm [46] to obtain the user association.
2) *MeanShift:* MeanShift [22] is a clustering-based method that deploys an UAV at the centroid of each cluster. It determines the number of UAVs solely based on the clustering result. However, it cannot adapt the UAV deployment according to the UEs' QoS requirements and backhaul capacity.
3) *K-Means:* K-means is a clustering-based algorithm that minimizes the within-cluster squared Euclidean distance [47] and allows for a predefined number of UAVs.
4) *Kuhn Munkres-K-Means:* We determine the UAV locations using the K-means algorithm according to the UEs' distribution, and we use the Kuhn Munkres-based algorithm [48] to obtain the user association.

In the simulations, the benchmark schemes fix the altitude of all the UAVs as $u^z_{j,\min}$ and determine the UAV selection, user association, and UAV locations using the corresponding algorithms. Then, the subproblems of UAV transmit power and bandwidth allocation are optimized using Step 3 of Algorithms 1 and 2 under the QoS and backhaul constraints.

A. System Cost Minimization Results

Fig. 3 shows the convergence result of the proposed Algorithm 1 for the system cost minimization with various numbers of UEs. Specifically, we deploy $K = 30$, 40, 50, and 60 UEs in a 500m $\times$ 500m square area, respectively. The weight of the UAV deployment cost is fixed as $\lambda_1 = 1$. The results show that Algorithm 1 converges in about eight iterations under different numbers of UEs.

Fig. 4 shows the selection and 3-D deployment of UAVs using Algorithm 1 for a specific UE distribution. In this scenario, 50 UEs marked by "$\times$" are randomly distributed within 500m $\times$ 500m square area. The GBS is marked by "$\blacklozenge$." To initialize a virtual set of UAVs, we employ a grid discretization method that selects seven grid intersection points as the initial locations of the UAVs that are marked by "Δ" and "$\star$." Algorithm 1 determines the deployed set of UAVs, their assignments to UEs, and their locations. The inactive UAVs that do not need to be deployed are marked by Δ, while the active UAVs are marked by "$\star$." The final locations of the active UAVs are marked by "$\star$." UEs associated with each active UAV are marked with the same color. The arrows point from the initial locations of the active UAVs to their final locations. Intending to minimize the system cost, Algorithm 1 jointly determines the selection and 3-D deployment of UAVs with the corresponding UE associations.

Numerical results from the Monte Carlo simulations are compared with the benchmark methods for randomly distributed UEs with varying numbers in a 500m $\times$ 500m square area. The evaluation is based on the results of 100 experiments. In Fig. 5, the curve and bar represent the system and UAV deployment costs, respectively. To verify the satisfaction of the QoS and backhaul constraints, we calculate the average backhaul utilization and the data rate to the QoS requirement ratio from the experiments with varying numbers of UEs. The results are summarized in Table III. The backhaul utilization

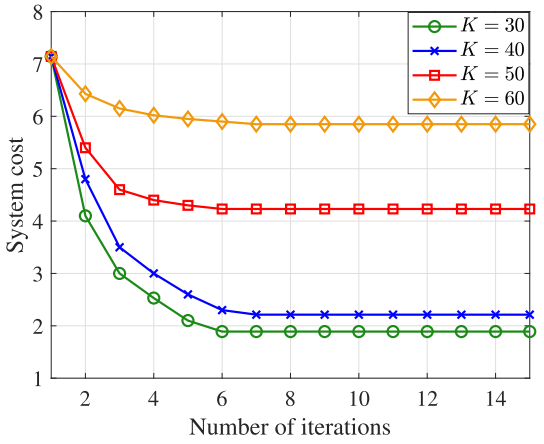

Fig. 3. Convergence result of Algorithm 1 for various numbers of UEs K, QoS requirement $\Gamma_k = 0.1$ Mb/s $\forall k \in \mathcal{K}$.

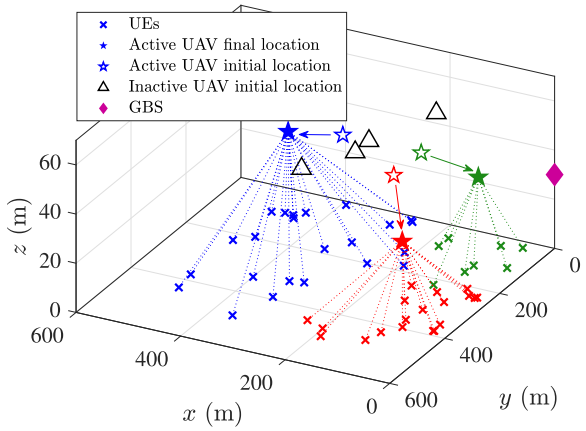

Fig. 4. Selection and 3-D deployment of UAVs with corresponding UE association using Algorithm 1 for a specific UE distribution with a virtual set of UAVs initialized as $J = 7$, number of UEs $K = 50$, and QoS requirement $\Gamma_k = 0.1$ Mb/s $\forall k \in \mathcal{K}$.

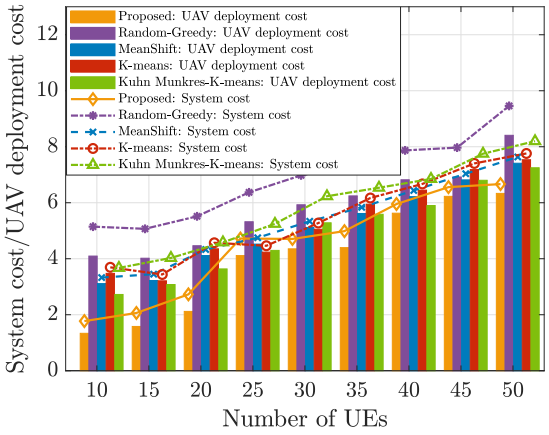

Fig. 5. Comparison of the average UAV deployment costs and system costs for different deployment methods, QoS requirement $\Gamma_k = 0.1$Mb/s $\forall k \in \mathcal{K}$.

TABLE III
BACKHAUL AND QOS CONSTRAINT VALIDATION FOR ALGORITHM 1

Method	NUE	BU (%)	BV	QoSR (%)	QoSV
Proposed	10	70.9	×	116.5	×
	20	71.8	×	118.9	×
	30	72.2	×	120.9	×
	40	71.5	×	123.2	×
	50	72.9	×	123.8	×
Random-Greedy	10	61.2	×	113.2	×
	20	62.9	×	117.5	×
	30	63.1	×	115.9	×
	40	58.9	×	119.6	×
	50	56.1	×	120.7	×
MeanShift	10	65.5	×	120.9	×
	20	66.0	×	121.2	×
	30	65.9	×	122.4	×
	40	63.4	×	124.5	×
	50	62.2	×	125.6	×
K-means	10	62.5	×	119.2	×
	20	64.6	×	120.1	×
	30	63.9	×	118.9	×
	40	60.2	×	121.3	×
	50	59.8	×	123.5	×
Kuhn Munkres-K-means	10	64.1	×	121.5	×
	20	65.6	×	121.9	×
	30	63.1	×	119.9	×
	40	61.4	×	124.6	×
	50	60.1	×	126.5	×

*NUE: number of UEs; BU: backhaul utilization; BV: backhaul violation; QoSR: data rate/QoS requirement ratio; QoSV: QoS requirement violation.

is always lower than 100%, and the data rate to the QoS requirement ratio is higher than 100% with no outage. Hence, all the methods satisfy the backhaul and QoS constraints. If the number of users is small, we can see that Algorithm 1 significantly reduce the system cost compared to the other four benchmark methods. For example, our proposed method can reduce more than 50% of the UAV deployment cost and the system cost when $K = 10, 15$. The cost reduction effect decreases as the number of users increases because more UAVs need to be deployed to meet the communication requirements of more UEs.

Fig. 6 shows the system cost under different deployment methods against the QoS requirements with different backhaul attenuation rates $\gamma = 0$ and 30dB/km. We distribute 30 UEs in a square area of 500m × 500m, and we can see that as the QoS requirements increase, the system cost of the three methods

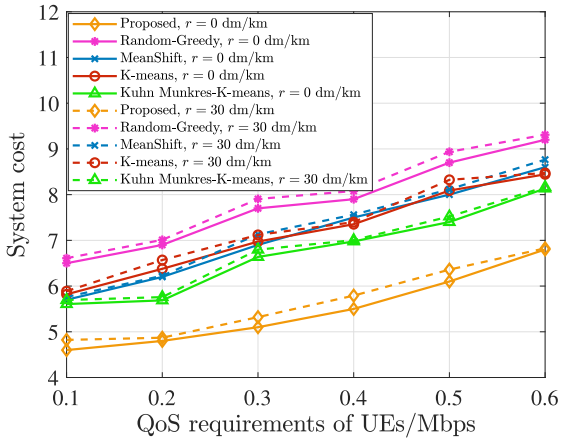

Fig. 6. System cost under different deployment methods for various QoS requirements Γ_k $\forall k \in \mathcal{K}$ with backhaul attenuation rates $\gamma = 0$ and 30dB/km.

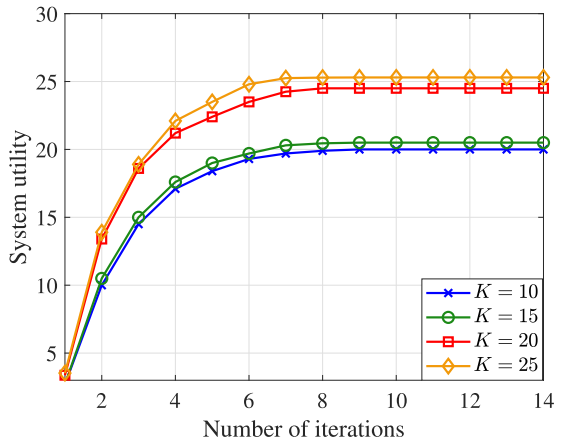

Fig. 7. Convergence result of Algorithm 2 for various numbers of UEs K.

gradually increases. This is because more UAVs need to be deployed to serve the UEs with the increased QoS, resulting in increased system costs. Fig. 6 demonstrates that Algorithm 1 achieves significantly lower system cost and exhibits good robustness under different QoS requirements. Even under high QoS and backhaul constraints, our proposed algorithm still reduces over 12% in the system costs compared to the best-performing benchmark method, i.e., Kuhn Munkres-K-means.

B. System Utility Maximization Results

For the system utility maximization problem, Fig. 7 shows the convergence result of the proposed Algorithm 2 for different numbers of UEs. Specifically, we deploy $K = 10$, 15, 20, and 25 UEs in a 500m × 500m square area, respectively. The weight of the UAV deployment cost is $\lambda_4 = 0.5$. It is observed that Algorithm 2 can converge in about nine iterations.

Fig. 8 shows the selection and 3-D deployment of UAVs obtained by Algorithm 2 for a specific UE distribution. The GBS is marked by ⧫. Ten grid intersection points are the selected initial locations for UAVs. The inactive UAVs are marked by △. The initial locations of active UAVs are marked by ☆ and their final locations are marked by ⋆. The UEs associated with each active UAV are marked by the same color.

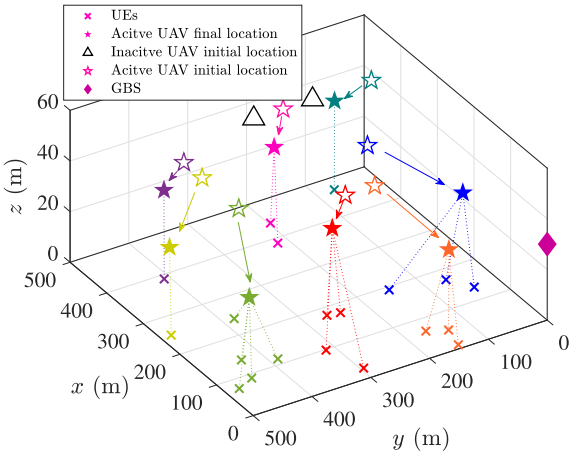

Fig. 8. Selection and 3-D deployment of UAVs with corresponding UE association using Algorithm 2 for a specific UE distribution. The set of UAVs is initialized as $J = 10$ with number of UEs $K = 20$.

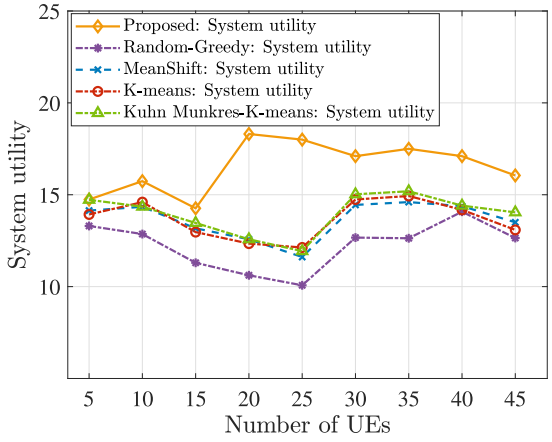

Fig. 9. Comparison of the average system utility for different deployment methods with varying numbers of UEs.

The arrows point from the initial locations of the active UAVs to their final locations.

Fig. 9 shows the average system utility of Algorithm 2 and the benchmark methods with varying numbers of UEs. The proposed and the benchmark methods are evaluated for randomly distributed UEs in a 500m × 500m square area based on the results of 100 experiments. The weight of the UAV deployment cost is set to $\lambda_4 = 1.5$. From Fig. 9, it is observed that Algorithm 2 achieves approximately 13%-30% higher system utility than other baseline methods. The average system utility does not exhibit a monotonic relationship with the number of UEs due to the incorporation of UAV deployment costs in the system utility calculation. Table IV shows that the QoS requirements and the backhaul constraints are satisfied by the results of Algorithm 2.

In Fig. 10, we compare the UAV deployment locations obtained by Algorithm 2 with the K-means method. We divide 20 UEs into two groups, resulting in the same association for both the methods. The K-means method deploys UAVs at the centroids of the UE clusters, whereas Algorithm 2 initially deploys one UAV at each group but continues to find their optimal final locations. In terms of communication, UAV

TABLE IV
BACKHAUL AND QOS CONSTRAINT VALIDATION FOR ALGORITHM 2

Method	NUE	BU (%)	BV	QoSR (%)	QoSV
Proposed	10	80.7	×	165.8	×
	20	78.4	×	164.5	×
	30	80.9	×	170.5	×
	40	81.6	×	177.5	×
	50	83.3	×	178.6	×
Random-Greedy	10	70.9	×	130.6	×
	20	72.7	×	132.6	×
	30	71.7	×	139.7	×
	40	70.3	×	131.9	×
	50	69.3	×	141.8	×
MeanShift	10	77.9	×	146.8	×
	20	79.8	×	148.6	×
	30	79.1	×	147.3	×
	40	78.4	×	158.6	×
	50	76.4	×	165.8	×
K-means	10	76.9	×	144.6	×
	20	78.4	×	146.6	×
	30	77.1	×	154.3	×
	40	76.8	×	154.6	×
	50	74.3	×	158.8	×
Kuhn Munkres-K-means	10	77.6	×	145.3	×
	20	79.6	×	147.6	×
	30	78.1	×	155.3	×
	40	76.8	×	156.3	×
	50	75.6	×	159.8	×

*NUE: number of UEs; BU: backhaul utilization; BV: backhaul violation; QoSR: data rate/QoS requirement ratio; QoSV: QoS requirement violation.

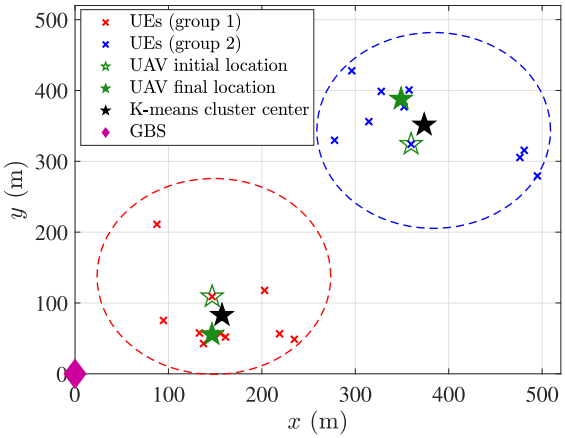

Fig. 10. Comparison of UAV deployment locations obtained by Algorithm 2 and the K-means method, number of UAV $J = 2$ and number of UEs $K = 20$.

deployment by Algorithm 2 is more effective at mitigating co-channel interference compared to the K-means method as evidenced by the higher system utility of 10.54 compared to 9.52 for the K-means method, where $\lambda_4 = 1.5$.

Fig. 11 shows the system utility against the number of UAVs under different backhaul attenuation rates (i.e., $\gamma = 0$ and 30dB/km). The ideal backhaul refers to the case that the backhaul capacity constraint (32c) is inactive. The results from Fig. 11 demonstrate that Algorithm 2 achieves significantly higher system utility compared to the other benchmarks with varying numbers of UAVs, because the UAVs in the benchmark schemes are deployed more distant from the GBS and the backhaul links are weak. Therefore, by optimizing the UAV deployment considering both the QoS and backhaul constraints, our proposed method can achieve the higher system utility than the benchmarks. Note that, the system utility of

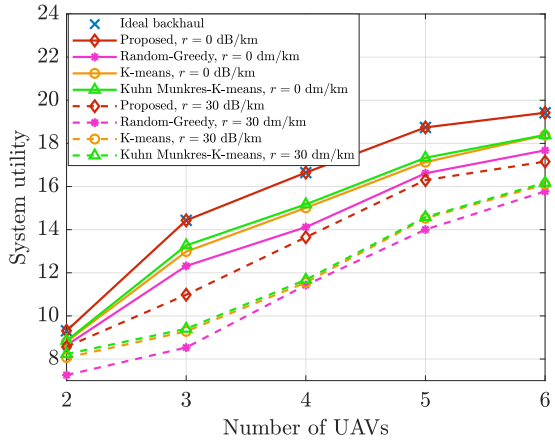

Fig. 11. System utility under different deployment methods with backhaul attenuation rates $\gamma = 0$ and 30 dB/km, and number of UEs $K = 20$.

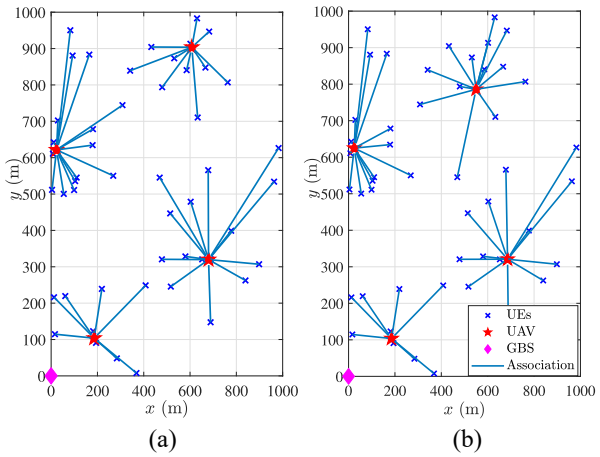

Fig. 12. Deployment of UAV with corresponding UE associations under different backhaul attenuation rates (a) $\gamma = 0$ and (b) 30 dB/km, number of UAV $J = 4$, and number of UEs $K = 50$.

all the algorithms is lower at $\gamma = 30$ compared to $\gamma = 0$. The reason is that there is a greater backhaul attenuation when $\gamma = 30$, resulting in lower backhaul transmission rates between the GBS and UAVs, thus affecting the whole system's utility. Fig. 11 further illustrates that Algorithm 2 effectively improves the system utility under different backhaul attenuation rates and varying numbers of UAVs, thereby validating the effectiveness of our proposed approach.

Fig. 12 shows the UAV deployment locations with the corresponding UE associations under different backhaul attenuations (i.e., $\gamma = 0$ and 30dB/km). In the figures, the GBS is marked by ♦, the UAVs are marked by ⋆, the UEs are marked by ×, and the blue lines represent the association between the UEs and the UAVs. Four UAVs provide communication services to 50 UEs randomly distributed in a 1000 m × 1000 m area. Results in Fig. 12(a) and (b) show that the proposed UE association dynamically adapts to the backhaul constraints with different backhaul attenuations. Specifically, when the backhaul attenuation rate is high (i.e., $\gamma = 30$ dB/km), the effective transmission distance of the GBS is limited. As a result, the UAV in the upper-right corner moves closer to the GBS to compensate for the constrained backhaul links.

Based on the simulation results, our proposed algorithms demonstrate significant improvements over the benchmark methods for the UAV-assisted wireless networks. Our algorithms take into account the impact of UAV deployment costs and backhaul capacity constraints, which are often overlooked in the previous studies. The proposed approaches yield solutions with lower system cost or higher system utility. Furthermore, our algorithms adaptively adjust the UAV locations and UAV-UE association strategies according to the available backhaul capacity, leading to improved communication performance.

The research results indicate that maintaining an optimal balance in UAV deployment is essential for achieving the network cost-effectiveness rather than merely maximizing the number of deployed UAVs. The insights highlight the importance of resource allocation efficiency, flexible adaptation to changing demands, and cost-benefit analyses. Network management should prioritize cost-effective solutions while ensuring adaptability to the dynamic requirements to achieve a balance between the service provision and UAV deployment costs.

VI. Conclusion

This article studies the system cost minimization and the system utility maximization problems in a multiple-UAV wireless network with the QoS and wireless backhaul constraints. Both the system cost and the system utility in the network take into account the UAV deployment cost, which is determined by the deployed UAV quantity. Joint optimization of the UAV selection, UAV-UE association, UAV locations, and wireless resource allocation is performed subject to the QoS requirements of UEs and the backhaul constraints. BCD methods combined with SCA are introduced to solve the complicated optimization problems efficiently. The designed algorithms effectively address the wireless backhaul constraints and perform better than the benchmark methods based on the geographical clustering. Simulation results highlight the superiority of the proposed algorithm compared to the benchmark methods when the QoS requirements and the backhaul constraints are present.

Our current analysis assumes the LoS channel model for the access links. However, the actual channel in an UAV network may be more complex. Therefore, investigating the network management approaches that consider realistic channel models for the UAV networks is an important topic for the future research. Additionally, our proposed methods are based on the mathematical optimization, which requires resolving the problem once the network setting changes. Obtaining solutions in real-time may be challenging in a highly dynamic UAV network. Therefore, we plan to explore neural network-based methods for more efficient solutions in our future work.

Appendix

Proof of Proposition 1 and 2

First, we define the function $G(x_1, \ldots, x_N) = \log(\sum_{n=1}^{N} \varepsilon_n x_n^{-1} + 1)$, $x_n > 0$, $\varepsilon_n > 0$. The Hessian matrix of $G(x_1, \ldots, x_N)$ is expressed as follows:

$$\mathbf{H} = \begin{bmatrix} H_1 & & & \\ & H_2 & & \\ & & \ddots & \\ & & & H_N \end{bmatrix} + \begin{bmatrix} \mu_1\mu_1 & \cdots & \cdots & \mu_1\mu_N \\ \vdots & \ddots & & \vdots \\ \vdots & & \ddots & \vdots \\ \mu_N\mu_1 & \cdots & \cdots & \mu_N\mu_N \end{bmatrix} \triangleq \mathbf{H}_d + \boldsymbol{\mu}^{\mathrm{T}}\boldsymbol{\mu} \quad (63)$$

where $H_n = ([2\varepsilon_n^2 x_n^{-3}(\sum_{n=1}^{N} \varepsilon_n x_n^{-1} + 1)]/[(\sum_{n=1}^{N} \varepsilon_n x_n^{-1} + 1)^2])$, $n = 1, \ldots, N$, $\boldsymbol{\mu} = [\mu_1, \ldots, \mu_N]^{\mathrm{T}}$, and $\mu_n = (-\varepsilon_n x_n^{-2}/\sum_{n=1}^{N} \varepsilon_n x_n^{-1} + 1)$, $n = 1, \ldots, N$.

Since, H_n is diagonal and $H_n > 0$, $\mathbf{H}_d$ is positive definite. Moreover, considering that $\boldsymbol{\mu}^{\mathrm{T}}\boldsymbol{\mu}$ is positive definite, $\mathbf{H} = \mathbf{H}_d + \boldsymbol{\mu}^{\mathrm{T}}\boldsymbol{\mu}$ is positive definite. Hence, the function $G(x_1, \ldots, x_N)$ is a convex function. Due to its convexity, we can obtain a global lower bound of $G(x_1, \ldots, x_N)$ using the first-order Taylor expansion according to Lemma 1, i.e.,

$$\log\left(\sum_{n=1}^{N} \varepsilon_n x_n^{-1} + 1\right) \geq \log\left(\sum_{n=1}^{N} \varepsilon_n \left(x_n^{(t)}\right)^{-1} + 1\right) - \frac{1}{\ln 2\left(\sum_{n=1}^{N} \varepsilon_n \left(x_n^{(t)}\right)^{-1} + 1\right)} \sum_{n=1}^{N} \frac{\varepsilon_n \left(x_n - x_n^{(t)}\right)}{\left(x_n^{(t)}\right)^2}. \quad (64)$$

According to (64), we can obtain the lower bound of $\theta_k(\mathbf{s}_k, \mathbf{v}_k)$ in Proposition 1 and $\eta_k(\bar{\mathbf{s}}_k, \bar{\mathbf{v}}_k)$ in Proposition 2 by expanding their first term, respectively.

REFERENCES

[1] M. Mozaffari, W. Saad, M. Bennis, Y.-H. Nam, and M. Debbah, "A tutorial on UAVs for wireless networks: Applications, challenges, and open problems," *IEEE Commun. Surveys Tuts.*, vol. 21, no. 3, pp. 2334–2360, 3rd Quart., 2019.

[2] W. Mei, Q. Wu, and R. Zhang, "Cellular-connected UAV: Uplink association, power control and interference coordination," *IEEE Trans. Wireless Commun.*, vol. 18, no. 11, pp. 5380–5393, Nov. 2019.

[3] R. Amer, W. Saad, and N. Marchetti, "Mobility in the sky: Performance and mobility analysis for cellular-connected UAVs," *IEEE Trans. Commun.*, vol. 68, no. 5, pp. 3229–3246, May 2020.

[4] Y. Zeng, R. Zhang, and T. J. Lim, "Wireless communications with unmanned aerial vehicles: Opportunities and challenges," *IEEE Commun. Mag.*, vol. 54, no. 5, pp. 36–42, May 2016.

[5] S. Zhang, H. Zhang, B. Di, and L. Song, "Cellular UAV-to-X communications: Design and optimization for multi-UAV networks," *IEEE Trans. Wireless Commun.*, vol. 18, no. 2, pp. 1346–1359, Feb. 2019.

[6] F. Cheng, G. Gui, N. Zhao, Y. Chen, J. Tang, and H. Sari, "UAV-relaying-assisted secure transmission with caching," *IEEE Trans. Commun.*, vol. 67, no. 5, pp. 3140–3153, May 2019.

[7] Q. Zhu, F. Bai, M. Pang, J. Li, W. Zhong, X. Chen, and K. Mao, "Geometry-based stochastic line-of-sight probability model for A2G channels under urban scenarios," *IEEE Trans. Antennas Propag.*, vol. 70, no. 7, pp. 5784–5794, Jul. 2022.

[8] D. Ebrahimi, S. Sharafeddine, P.-H. Ho, and C. Assi, "UAV-aided projection-based compressive data gathering in wireless sensor networks," *IEEE Internet Things J.*, vol. 6, no. 2, pp. 1893–1905, Apr. 2019.

[9] M. Samir, S. Sharafeddine, C. M. Assi, T. M. Nguyen, and A. Ghrayeb, "UAV trajectory planning for data collection from time-constrained IoT devices," *IEEE Trans. Wireless Commun.*, vol. 19, no. 1, pp. 34–46, Jan. 2020.

[10] D.-Y. Kim, W. Saad, and J.-W. Lee, "On the use of high-rise topographic features for optimal aerial base station placement," *IEEE Trans. Wireless Commun.*, vol. 22, no. 3, pp. 1868–1884, Mar. 2023.

[11] C.-C. Lai, C.-T. Chen, and L.-C. Wang, "On-demand density-aware UAV base station 3D placement for arbitrarily distributed users with guaranteed data rates," *IEEE Wireless Commun. Lett.*, vol. 8, no. 3, pp. 913–916, Jun. 2019.

[12] X.-R. Xu, Y.-H. Xu, W. Zhou, and A. Nallanathan, "Energy efficient resource allocation for UAV-served energy harvesting-supported cognitive industrial M2M networks," *IEEE Wireless. Commun. Lett.*, vol. 12, no. 8, pp. 1454–1458, Aug. 2023.

[13] Y. Liu, Q. Wang, H.-N. Dai, Y. Fu, N. Zhang, and C. C. Lee, "UAV-assisted wireless backhaul networks: Connectivity analysis of uplink transmissions," *IEEE Trans. Veh. Technol.*, vol. 72, no. 9, pp. 12195–12207, Sep. 2023.

[14] A. Mahmood, T. X. Vu, S. Chatzinotas, and B. Ottersten, "Joint optimization of 3D placement and radio resource allocation for per-UAV sum rate maximization," *IEEE Trans. Veh. Technol.*, vol. 72, no. 10, pp. 13094–13105, Oct. 2023.

[15] N. Lin, Y. Liu, L. Zhao, D. O. Wu, and Y. Wang, "An adaptive UAV deployment scheme for emergency networking," *IEEE Trans. Wireless Commun.*, vol. 21, no. 4, pp. 2383–2398, Apr. 2022.

[16] P. Chen, X. Zhou, J. Zhao, F. Shen, and S. Sun, "Energy-efficient resource allocation for secure D2D communications underlaying UAV-enabled networks," *IEEE Trans. Veh. Technol.*, vol. 71, no. 7, pp. 7519–7531, Jul. 2022.

[17] S. Lhazmir, O. A. Oualhaj, A. Kobbane, and J. Ben-Othman, "Matching game with no-regret learning for IoT energy-efficient associations with UAV," *IEEE Trans. Green Commun*, vol. 4, no. 4, pp. 973–981, Dec. 2020.

[18] X. Huo, H. Zhang, Z. Wang, H. Yan, and C. Liu, "An efficient matching game approach to association formation in UAV-enabled hierarchical distributed learning," *IEEE Trans. Cybern.*, early access, Feb. 15, 2024, doi: 10.1109/TCYB.2024.3357848.

[19] S. Zhou, Y. Cheng, X. Lei, Q. Peng, J. Wang, and S. Li, "Resource allocation in UAV-assisted networks: A clustering-aided reinforcement learning approach," *IEEE Trans. Veh. Technol.*, vol. 71, no. 11, pp. 12088–12103, Nov. 2022.

[20] Z. Kang, C. You, and R. Zhang, "Placement learning for multi-UAV relaying: A Gibbs sampling approach," in *Proc. IEEE Int. Conf. Commun. (ICC)*, Dublin, Ireland, 2020, pp. 1–6.

[21] H. Dai, H. Zhang, M. Hua, C. Li, Y. Huang, and B. Wang, "How to deploy multiple UAVs for providing communication service in an unknown region?" *IEEE Wireless Commun. Lett.*, vol. 8, no. 4, pp. 1276–1279, Aug. 2019.

[22] I. Valiulahi and C. Masouros, "Multi-UAV deployment for throughput maximization in the presence of co-channel interference," *IEEE Internet Things J.*, vol. 8, no. 5, pp. 3605–3618, Mar. 2021.

[23] J. Sun and C. Masouros, "Deployment strategies of multiple aerial BSs for user coverage and power efficiency maximization," *IEEE Trans. Commun.*, vol. 67, no. 4, pp. 2981–2994, Apr. 2019.

[24] L. Wang, H. Zhang, S. Guo, and D. Yuan, "Deployment and association of multiple UAVs in UAV-assisted cellular networks with the knowledge of statistical user position," *IEEE Trans. Wireless Commun.*, vol. 21, no. 8, pp. 6553–6567, Aug. 2022.

[25] Z. Gao, L. Dai, D. Mi, Z. Wang, M. A. Imran, and M. Z. Shakir, "Mmwave massive-MIMO-based wireless backhaul for the 5G ultra-dense network," *IEEE Wireless Commun.*, vol. 22, no. 5, pp. 13–21, Oct. 2015.

[26] W. Du, T. Wang, H. Zhang, D. Wu, and Y. Li, "Resource allocation for the backhaul of NOMA-based cellular UAV network," *IEEE Trans. Veh. Technol.*, vol. 71, no. 11, pp. 11889–11899, Nov. 2022.

[27] B. Hu, L. Wang, S. Chen, J. Cui, and L. Chen, "An uplink throughput optimization scheme for UAV-enabled urban emergency communications," *IEEE Internet Things J.*, vol. 9, no. 6, pp. 4291–4302, Mar. 2022.

[28] C.-C. Lai, L.-C. Wang, and Z. Han, "Data-driven 3D placement of UAV base stations for arbitrarily distributed crowds," in *Proc. IEEE Global Commun. Conf. (GLOBECOM)*, Waikoloa, HI, USA, 2019, pp. 1–6.

[29] H. El Hammouti, M. Benjillali, B. Shihada, and M.-S. Alouini, "Learn-as-you-fly: A distributed algorithm for joint 3D placement and user association in multi-UAVs networks," *IEEE Trans. Wireless Commun.*, vol. 18, no. 12, pp. 5831–5844, Dec. 2019.

[30] C. Qiu, Z. Wei, X. Yuan, Z. Feng, and P. Zhang, "Multiple UAV-mounted base station placement and user association with joint fronthaul and backhaul optimization," *IEEE Trans. Commun.*, vol. 68, no. 9, pp. 5864–5877, Sep. 2020.

[31] M. Banagar and H. S. Dhillon, "3D two-hop cellular networks with wireless backhauled UAVs: Modeling and fundamentals," *IEEE Trans. Wireless Commun.*, vol. 21, no. 8, pp. 6417–6433, Aug. 2022.

[32] M. Hong, M. Razaviyayn, Z.-Q. Luo, and J.-S. Pang, "A unified algorithmic framework for block-structured optimization involving big data: With applications in machine learning and signal processing," *IEEE Signal Process Mag.*, vol. 33, no. 1, pp. 57–77, Jan. 2016.

[33] D. Bethanabhotla, O. Y. Bursalioglu, H. C. Papadopoulos, and G. Caire, "User association and load balancing for cellular massive MIMO," in *Proc. Inf. Theory Appl. Workshop (ITA)*, San Diego, CA, USA, 2014, pp. 1–10.
[34] N. Wang, E. Hossain, and V. K. Bhargava, "Joint downlink cell association and bandwidth allocation for wireless backhauling in two-tier HetNets with large-scale antenna arrays," *IEEE Trans. Wireless Commun.*, vol. 15, no. 5, pp. 3251–3268, May 2016.
[35] W. Feng, Y. Li, D. Jin, L. Su, and S. Chen, "Millimetre-wave backhaul for 5G networks: Challenges and solutions," *Sensors.*, vol. 16, no. 6, p. 892, Jun. 2016.
[36] Z. Qingling and J. Li, "Rain attenuation in millimeter wave ranges," in *Proc. 7th Int. Symp. Antennas, Propag. EM Theory (ISAPE)*, Guilin, China, 2006, pp. 1–4.
[37] Q. Wu, Y. Zeng, and R. Zhang, "Joint trajectory and communication design for multi-UAV enabled wireless networks," *IEEE Trans. Commun.*, vol. 17, no. 3, pp. 2109–2121, Mar. 2018.
[38] Y. Sun, D. Xu, D. W. K. Ng, L. Dai, and R. Schober, "Optimal 3D-trajectory design and resource allocation for solar-powered UAV communication systems," *IEEE Trans. Commun.*, vol. 67, no. 6, pp. 4281–4298, Jun. 2019.
[39] C. E. Shannon, "A mathematical theory of communication," *Bell Syst. Tech. J.*, vol. 27, no. 3, pp. 379–423, Jul. 1948.
[40] Y. Xu and W. Yin, "A block coordinate descent method for regularized multiconvex optimization with applications to nonnegative tensor factorization and completion," *SIAM J. Imag. Sci.*, vol. 6, no. 3, pp. 1758–1789, 2013.
[41] B. R. Marks and G. P. Wright, "A general inner approximation algorithm for nonconvex mathematical programs," *Oper. Res.*, vol. 26, no. 4, pp. 681–683, Jul. 1978.
[42] S. Boyd and L. Vandenberghe, *Convex Optimization*. Cambridge, U.K.: Cambridge Univ., 2004.
[43] M. Grant and S. Boyd. "CVX: MATLAB software for disciplined convex programming, version 2.2." 2020. [Online]. Available: https://cvxr.com/cvx
[44] M. Razaviyayn, M. Hong, and Z.-Q. Luo, "A unified convergence analysis of block successive minimization methods for nonsmooth optimization," *SIAM J. Optim.*, vol. 23, no. 2, pp. 1126–1153, 2013.
[45] J. Zhao, T. Q. Quek, and Z. Lei, "Coordinated multipoint transmission with limited backhaul data transfer," *IEEE Trans. Wireless Commun.*, vol. 12, no. 6, pp. 2762–2775, Jun. 2013.
[46] J. Wang, C. Jiang, Z. Han, Y. Ren, R. G. Maunder, and L. Hanzo, "Taking drones to the next level: Cooperative distributed unmanned-aerial-vehicular networks for small and mini drones," *IEEE Veh. Technol. Mag.*, vol. 12, no. 3, pp. 73–82, Sep. 2017.
[47] D. Arthur and S. Vassilvitskii, "K-means++: The advantages of careful seeding," in *Proc. ACM-SIAM Symp. Discrete Algorithms (SODA)*, New Orleans, LA, USA, 2007, pp. 1027–1035.
[48] H. El Hammouti, D. Hamza, B. Shihada, M.-S. Alouini, and J. S. Shamma, "The optimal and the greedy: Drone association and positioning schemes for Internet of UAVs," *IEEE Internet Things J.*, vol. 8, no. 18, pp. 14066–14079, Sep. 2021.

Shengqi Geng received the B.S. degree from the School of Microelectronics and Communication Engineering, Chongqing University, Chongqing, China, in 2022. He is currently pursuing the master's degree with the School of Electronic Science and Engineering, Nanjing University, Nanjing, China.

His research interests include UAV communication and wireless communication networks optimization.

Zhe Wei received the B.S. degree from the School of Electronic Science and Engineering and the M.S. degree from Nanjing University, Nanjing, China, in 2019 and 2022, respectively.

His research interests include resource management for wireless communication networks.

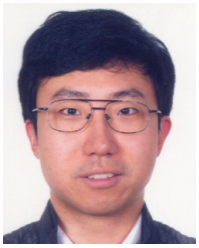

Jian Zhao (Senior Member, IEEE) received the B.S. degree from Nanjing University, Nanjing, China, in 2001, the M.Sc. degree from Hamburg University of Technology, Hamburg, Germany, in 2004, and the Dr.Sc. degree from Swiss Federal Institute of Technology, Zurich, Switzerland, in 2010.

From 2010 to 2015, he was a Research Scientist with the Institute for Infocomm Research, Agency for Science, Technology and Research, Singapore. He is currently an Associate Professor with the School of Electronic Science and Engineering, Nanjing University. His research interests include next-generation wireless communication networks, deep learning, and mathematical optimization techniques.

Dr. Zhao was honored with the Dengfeng Scholars Program of Nanjing University in 2015, the 2009 Chinese Government Award for Outstanding Self-Financed Students Abroad, and the IEEE Globecom 2008 Best Paper Award.

Furao Shen (Member, IEEE) received the B.Sc. and M.Sc. degrees in mathematics from Nanjing University, Nanjing, China, in 1995 and 1998, respectively, and the Ph.D. degree from Tokyo Institute of Technology, Tokyo, Japan, in 2006.

He is currently a Full Professor with the School of Artificial Intelligence, Nanjing University. His current research interests include neural computing and robotic intelligence.

Jingon Joung (Senior Member, IEEE) received the B.S. degree in radio communication engineering from Yonsei University, Seoul, South Korea, in 2001, and the M.S. and Ph.D. degrees in electrical engineering and computer science from Korea Advanced Institute of Science and Technology (KAIST), Daejeon, South Korea, in 2003 and 2007, respectively.

He was a Postdoctoral Fellow with KAIST in 2007 and University of California at Los Angeles, Los Angeles, CA, USA, in 2008. He was a Scientist with the Institute for Infocomm Research, Singapore, from 2009 to 2015, and joined Chung-Ang University (CAU), Seoul, in 2016, as a Faculty Member. He is currently a Professor with the School of Electrical and Electronics Engineering, CAU, where he is also the Principal Investigator of the Intelligent Wireless Systems Lab and Next-Generation Intelligent Sensing and Communication Lab. He is an Inventor of a Space-Time Line Code that is a fully symmetric scheme to a space-time block code. His research interests include signal processing, numerical analysis, and algorithms.

Dr. Joung was recognized as an Exemplary Reviewer of IEEE COMMUNICATIONS LETTERS in 2012 and IEEE WIRELESS COMMUNICATIONS LETTERS from 2012 to 2014 and in 2019. He served as the Guest Editor for IEEE ACCESS in 2016. He served on the editorial board for APSIPA TRANSACTIONS ON SIGNAL AND INFORMATION PROCESSING from 2014 to 2019, as a Guest Editor for ELECTRONICS in 2019, and as an Associate Editor for IEEE TRANSACTIONS ON VEHICULAR TECHNOLOGY from 2018 to 2023 (Top Editor 2021).

Sumei Sun (Fellow, IEEE) received the B.Sc. degree from Peking University, Beijing, China, the M.Eng. degree from Nanyang Technological University, Singapore, and the Ph.D. degree from National University of Singapore, Singapore.

She is the Executive Director of the Institute for Infocomm Research (I^2R), Agency for Science, Technology, and Research, Singapore. She holds an adjunct appointment with the National University of Singapore and a joint appointment with Singapore Institute of Technology both as a Full Professor. Her current research interests include next-generation wireless communications, joint communication-sensing-computing-control design, industrial Internet of Things, applied deep learning, and artificial intelligence.

Prof. Sun was the Editor-in-Chief of IEEE OPEN JOURNAL OF VEHICULAR TECHNOLOGY from 2019 to 2023. She is a member of the IEEE Vehicular Technology Society Board of Governors from 2022 to 2024 and a Fellow of the Academy of Engineering Singapore.